

pubs.acs.org/JCTC Article

# Quantum Circuit and Mapping Algorithms for Wavepacket Dynamics: Case Study of Anharmonic Hydrogen Bonds in Protonated and Hydroxide Water Clusters

Debadrita Saha, Philip Richerme, and Srinivasan S. Iyengar\*



Cite This: J. Chem. Theory Comput. 2025, 21, 3814–3831



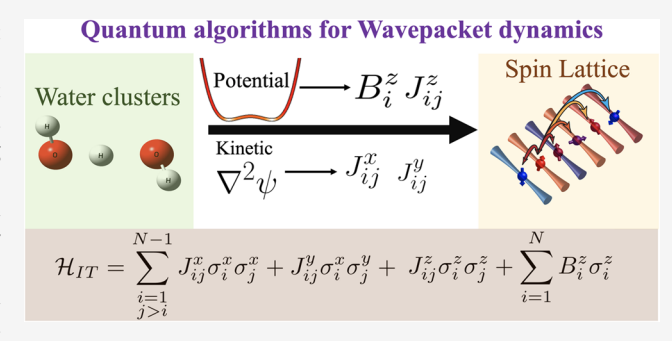
ACCESS I

III Metrics & More

Article Recommendations

Supporting Information

ABSTRACT: The accurate computational study of wavepacket nuclear dynamics is considered to be a classically intractable problem, particularly with increasing dimensions. Here, we present two algorithms that, in conjunction with other methods developed by us, may result in one set of contributions for performing quantum nuclear dynamics in arbitrary dimensions. For one of the two algorithms discussed here, we present a direct map between the Born-Oppenheimer Hamiltonian describing the nuclear wavepacket time evolution and the control parameters of a spin-lattice Hamiltonian that describes the dynamics of qubit states in an ion-trap quantum computer. This map is exact for three qubits, and when implemented, the dynamics of the spin states emulates those



of the nuclear wavepacket in a continuous representation. However, this map becomes approximate as the number of qubits grows. In a second algorithm, we present a general quantum circuit decomposition formalism for such problems using a method called the Quantum Shannon Decomposition. This algorithm is more robust and is exact for any number of qubits at the cost of increased circuit complexity. The resultant circuit is implemented on IBM's quantum simulator (QASM) for 3–7 qubits, without using a noise model so as to test the intrinsic accuracy of the method. In both cases, the wavepacket dynamics is found to be in good agreement with the classical propagation result and the corresponding vibrational frequencies obtained from the wavepacket density time evolution are in agreement to within a few tenths of a wavenumber.

### I. INTRODUCTION

Protonated, <sup>1–3</sup> neutral, <sup>4</sup> and hydroxide-rich water clusters <sup>5–10</sup> have been widely studied, both experimentally <sup>11–15</sup> and theoretically <sup>16–19</sup> due to their broad significance in multiple areas including atmospheric, <sup>20–22</sup> biological, <sup>23–27</sup> and condensed phase chemistry. <sup>28,29</sup> Substantial efforts have been devoted to understanding the relatively high efficiency of organic reactions on the surface of water droplets. <sup>30–48</sup> Additionally, protonated water clusters in polymer electrolyte membrane fuel cells <sup>49,50</sup> are thought to mediate proton transfer.

Experimental studies on vibrational properties of such hydrogen-bonded cluster systems have blossomed due to the development of sophisticated cluster-based measurement techniques such as argon-tagged single-photon action spectral methods<sup>51</sup> and the infrared multiple photon dissociation (IRMPD)<sup>52</sup> approach. Both gas-phase single-photon<sup>51,53</sup> and multiple photon<sup>52,54–57</sup> vibrational action spectroscopic techniques have been crucial in deciphering the precise signatures that contribute to dynamics and spectroscopy in hydrogen-bonded systems. However, the accurate computational modeling of the processes involved in these experiments requires both the quantum mechanical treatment of electronic

and nuclear motion. \$3,58-61 Due to the light mass of the transferring proton involved in such hydrogen-bonded systems, these systems often exhibit quantum effects such as hydrogen tunneling and zero point energy, \$62-68\$ and the correlated behavior of multiple nuclear degrees of freedom. \$3,58,59,61,69-77\$ In such scenarios, classical approaches such as approximating nuclear motion to be harmonic about the equilibrium geometry \$78,79\$ fail to accurately predict the static and dynamic properties of such hydrogen-bonded systems. \$1,53,58,80,81\$ A full quantum mechanical treatment of the nuclear degrees of freedom and its associated electronic interactions is often needed \$8-60,75,76,82\$ to account for such quantum nuclear effects, including multidimensional effects, in the computation of their molecular properties. This then requires the computation of potential energy surfaces for describing the nuclear degrees of freedom in such systems and the explicit

Received: October 8, 2024 Revised: March 5, 2025 Accepted: March 6, 2025 Published: April 2, 2025





time evolution of the quantum nuclear wavepacket on the potential landscape. However, the study of such multidimensional quantum nuclear processes is complicated by (a) the steep algebraic computational scaling of accurate electron correlation methods  $^{83}$  and (b) the exponential scaling of quantum nuclear dynamics with the number of quantum nuclear degrees of freedom.  $^{84-96}$ 

Over the years, several classical algorithms have been developed to improve the computational scaling of electronic<sup>97–101</sup> and nuclear dynamics<sup>86,102–106</sup> problems. Orthogonally, recent years have also seen the development of quantum computing algorithms for performing electronic structure calculations on near-term quantum hardware. 107-117 These have been complemented by state-of-the-art experiments<sup>118–124</sup> for strongly correlated electrons. In addition, quantum simulations of vibronic spectra, <sup>125–128</sup> wavepacket evolution through conical intersections, <sup>129–134</sup> and algorithms for reduced-dimensional reactive scattering studies 135,136 have also been undertaken. However, the work in refs 125-134 invokes the harmonic approximation for nuclear dynamics which, as stated above, does not appropriately describe quantum nuclear effects within hydrogen-bonded systems emanating from anharmonic effects and mode-coupling effects. 1-3,51,53,81,137 The treatment of nuclear quantum wavepacket dynamics on anharmonic potential surfaces through quantum algorithms and through quantum hardware, that also include multidimensional mode-coupling effects, has received very little attention. This paper, along with refs 138-141 are an important step in the direction of treating anharmonic hydrogen-bonded systems. To the best of our knowledge, refs 138-140 are the only studies on this topic to

In ref 138, a Hamiltonian mapping protocol was introduced to simulate the quantum nuclear dynamics in proton transfer reactions on spin—lattice quantum simulators. This was successfully implemented on Sandia National Laboratories' Quantum Scientific Computing Open User Testbed (QSCOUT) ion-trap system<sup>139</sup> to study the vibrational signatures of the transferring proton in a short, strong hydrogen-bonded system. An improvement of this scheme to higher nuclear dimensions using a tensor-network-based formalism was discussed in refs 140,142. A method to perform a parallel quantum computation of quantum wavepacket dynamics on a distributed set of ion-trap systems, along with implementation on IonQ's 11-qubit Harmony ion-trap quantum systems is discussed in ref 140.

Quantum algorithms for simulating processes on quantum simulators can be broadly divided into two major classes: Hamiltonian (analogue) quantum simulation and unitary or quantum circuit decomposition (digital). In this paper, we discuss both an analog Hamiltonian-based and a quantum circuit decomposition-based algorithm to study spectroscopic features arising from anharmonic vibrations in small water clusters using quantum wavepacket dynamics. Hamiltonian or analogue quantum simulation proceeds by mapping a desired Hamiltonian to the Hamiltonian of the quantum device. This is done by programming the control parameters of the quantum device Hamiltonian. The mapping protocol discussed here 138,139 simulates a chemical dynamics Hamiltonian on an ion-trap quantum computer by computing the control parameters for an Ising Hamiltonian, which describes the dynamics of ions in the ion lattice. As a result, the ion lattice dynamics directlycorresponds to the dynamics of the chemical

system. The mapping protocol, however, is inherently approximate and only works well for systems with specific symmetries and for a small number of qubits; errors grow with an increasing number of qubits in this algorithm. Quantum circuit decomposition is more commonly used to write the unitary time evolution operator corresponding to the Hamiltonian of a system in terms of universal quantum gate sets. The circuit model, in theory, can be extended to an arbitrary number of qubits but suffers from increased circuit depth and an exponentially increasing number of entangling gates as we scale up to a higher number of qubits. This results in increased measurement errors and loss of contrast in the measured probabilities due to the low fidelities of the entangling gates. For a more accurate implementation of quantum nuclear dynamics problems, we discuss a quantum circuit model-based approach to studying wavepacket dynamics. This decomposition technique is based on Quantum Shannon Decomposition (QSD). 143 Notably, Quantum Shannon Decomposition achieves CNOT gate counts closest to the theoretical lower bound. 143 The decomposition is a recursive gate decomposition technique, where at each recursion the unitary operations are decomposed into known quantum gate structures like the quantum multiplexors and multicontrolled rotation gates. These quantum gate intermediates have efficient gate decompositions in terms of universal quantum sets that can be implemented on quantum hardware. This algorithm is implemented for the first time here for a chemical dynamics problem using a Qiskit simulator.

This article is organized as follows: In Section II, we discuss the Hamiltonian mapping protocol that was developed in ref 138. This approach is exact for three qubits but becomes approximate as the number of qubits grow. Hence, in Section III, we outline the Quantum Shannon circuit decomposition technique that is used to decompose the unitary propagator corresponding to the nuclear Hamiltonian. The algorithm presented in Section III yields a quantum circuit with the number of entanglement gates close to the theoretical lower bound 143 and works for an arbitrary number of qubits. Both techniques use the first quantized form of the nuclear Hamiltonian computed in a continuous (grid) representation. Numerical results are presented for both algorithms in Section IV B and IV C for the anharmonic molecular vibrations of the shared proton in short, strong hydrogen bonds<sup>27,144-146</sup> that are present in protonated and hydroxide-rich water clusters. These include explicit numerical propagation of the molecular dynamics problem, the mapped spin-lattice dynamics governed by Ising-type Hamiltonian as obtained from the mapping protocol, and quantum circuit decomposition using QSD. The Quantum Shannon Decomposition approach is implemented on Qiskit, and results from quantum simulation on a classical computer are provided here. No noise model is included in the Qiskit simulations to allow us to gauge the intrinsic accuracy of our circuit compilation technique. The systems considered in Section IV are the  $H_5O_2^+$  and  $H_3O_2^-$  ions. These low-barrier, short, strong hydrogen-bonded systems<sup>7-9,146-149</sup> are of fundamental significance in proton transfer processes and have a critical role in the enhanced mobility of protons and deuterons in condensed phase, in biological ion channels and enzymes, and in fuel cells. 150-153 We inspect the vibrational properties of these systems using the quantum algorithms presented here. Conclusions are given in Section V.

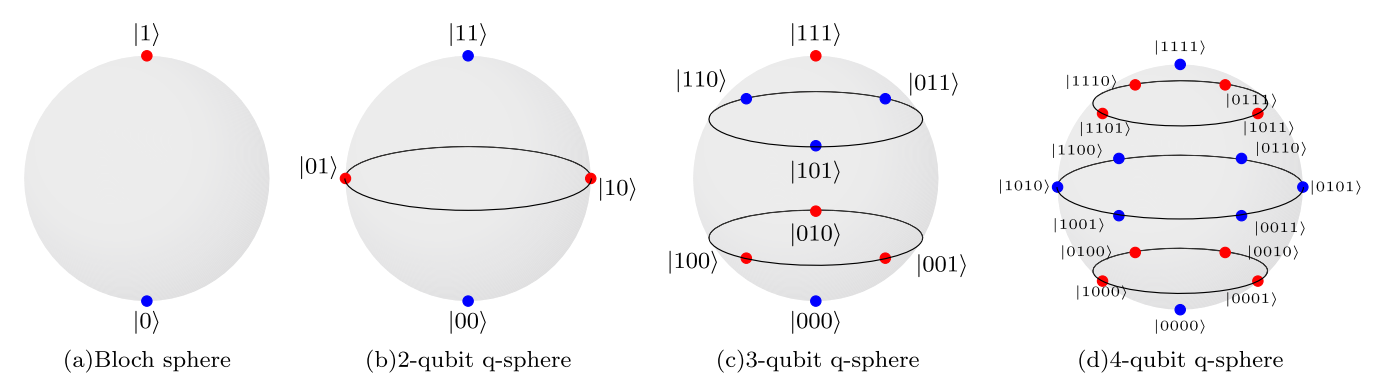


Figure 1. Generalized Bloch sphere for an arbitrary number of qubits, along with the classification of basis states, is shown using red and blue colors.

# II. QUANTUM ALGORITHMS FOR WAVEPACKET DYNAMICS: MAPPING PROTOCOLS FOR SPIN-LATTICE SIMULATIONS

The generalized form of the Ising Hamiltonian can be used to describe the interactions of spin states on a spin-lattice. The mapping protocol introduced in ref 138 relates a quantum nuclear Hamiltonian, involving the nuclear kinetic energy operator and the Born-Oppenheimer potential surface obtained from electronic structure theory, to a generalized Ising Hamiltonian realizable on a range of quantum systems including ion trap quantum simulators. The inherent symmetries of the Ising Hamiltonian that describe the dynamics of effective spin states on a lattice (outlined in Section II A) and that of the Born-Oppenheimer potential and nuclear kinetic energy (Section II B) are exploited to arrive at the map. In the following sections, we provide the transformations and their geometric interpretations that expose these symmetries in Ising (Section II A) and the nuclear Hamiltonian (Section II C). The parameters of the Ising Hamiltonian that are programmable on a lattice of ions are computed from the quantum nuclear Hamiltonian, and the algorithm is summarized in Section II C.

The mapping algorithm discussed here differs from mapping methods developed for electronic structure. 154 First, the mapping here pertains to quantum nuclear dynamics and hence, the Jordan-Wigner transformations<sup>155</sup> do not turn out to be applicable. Second, the Hamiltonian that describes wavepacket dynamics is introduced here in first quantized form to accurately represent all anharmonic effects in the Born-Oppenheimer potential energy surface. By contrast, the mapping protocols for electronic structure generally begin with a second quantized form of the Hamiltonian that includes the commutation properties of the corresponding field operators. A collection of nuclear degrees of freedom, on the other hand, may have Bosonic and Fermionic constituents. For example, the hydrogen nucleus is a Fermion, but Deuterium is a Boson. Additionally, the intrinsic spin statistics of nuclear degrees of freedom arising from permutation symmetries of the wave functions that describe the constituent nuclear degrees of freedom do not play a significant role under ambient conditions in biological, materials, and atmospheric systems. As a result, most such quantum dynamics studies are currently constructed on classical computing platforms using basis sets and on grids in first quantized form. 84,156,157 Our approach is applicable to the vast literature of quantum nuclear wavepacket dynamics work constructed using first quantization.

This section is organized as follows: The mapping algorithm that describes the connection between the generalized Ising model (eq 1) and a quantum nuclear Hamiltonian, which contains the nuclear kinetic energy operator and the electronic potential energy surface, was introduced in ref 138. The key aspects of this algorithm are based on the symmetry of Ising Hamiltonian. In Section II A, we present a geometric interpretation to arrive at these same symmetries, which is different from that discussed in ref 138. The mapping results are presented in Section II C along with a discussion of limitations. In Section III, we present the more general QSD formalism.

A. The Role of Geometric Structure in Generalized Ising Hamiltonians toward Achieving a Map to Quantum Nuclear Dynamics. Any two-level quantum system can be mapped to a spin-1/2 particle in an effective magnetic field. In the ion trap used in ref 139, the qubit levels encoded onto the  ${}^2S_{1/2}$  state, namely,  $|F=0,m_F=0\rangle$  and  $|F=1,m_F=0\rangle$  hyperfine "clock" states of  ${}^{171}\text{Yb}^+$  ions are mapped onto the two levels of a spin-1/2 particle and denoted as  $|0\rangle$  and  $|1\rangle$ , respectively.  ${}^{158}$  In its most generalized form, the Ising Hamiltonian that can be implemented on such an ion trap is given by,

$$\mathcal{H}_{IT} = \sum_{i=1}^{N-1} \sum_{j>i}^{N} \{ J_{ij}^{x} \sigma_{i}^{x} \sigma_{j}^{x} + J_{ij}^{y} \sigma_{i}^{y} \sigma_{j}^{y} + J_{ij}^{z} \sigma_{i}^{z} \sigma_{j}^{z} \}$$

$$+ \sum_{i=1}^{N} \{ B_{i}^{x} \sigma_{i}^{x} + B_{i}^{y} \sigma_{i}^{y} + B_{i}^{z} \sigma_{i}^{z} \}$$
(1)

where  $\{\sigma_i^x, \sigma_i^y, \sigma_i^z\}$  are the Pauli spin operators on the *i*-th lattice site along the respective spatial direction. The energy gap between the states at each ion, i, and their relative orientations are controlled by local effective magnetic fields,  $\{B_i^x, B_i^y, B_i^z\}$ , and the spin-spin coupling between different lattice sites, i and j, is controlled using laser pulses, also spatially nonisotropic, and represented as  $\{J_{ij}^x, J_{ij}^y, J_{ij}^z\}$ . It is critical to note that the expression above is more general than the form of the Ising Hamiltonian commonly used in condensed matter physics, <sup>159–161</sup> NMR, other zero-field splitting studies <sup>162</sup> where only nearest-neighbor interactions or spin-lattice sites within a certain spatial distance may interact and magnetic fields only across certain directions are considered, and transverse Ising models 163-165 implemented for adiabatic quantum computing for electronic structure studies. 154 The magnetic fields and intersite coupling parameters,  $\{J_{ii}^{\gamma}, B_{i}^{\gamma}\}$  with  $\gamma \in \{x, y, z\}$ , form a set of programmable parameters that can

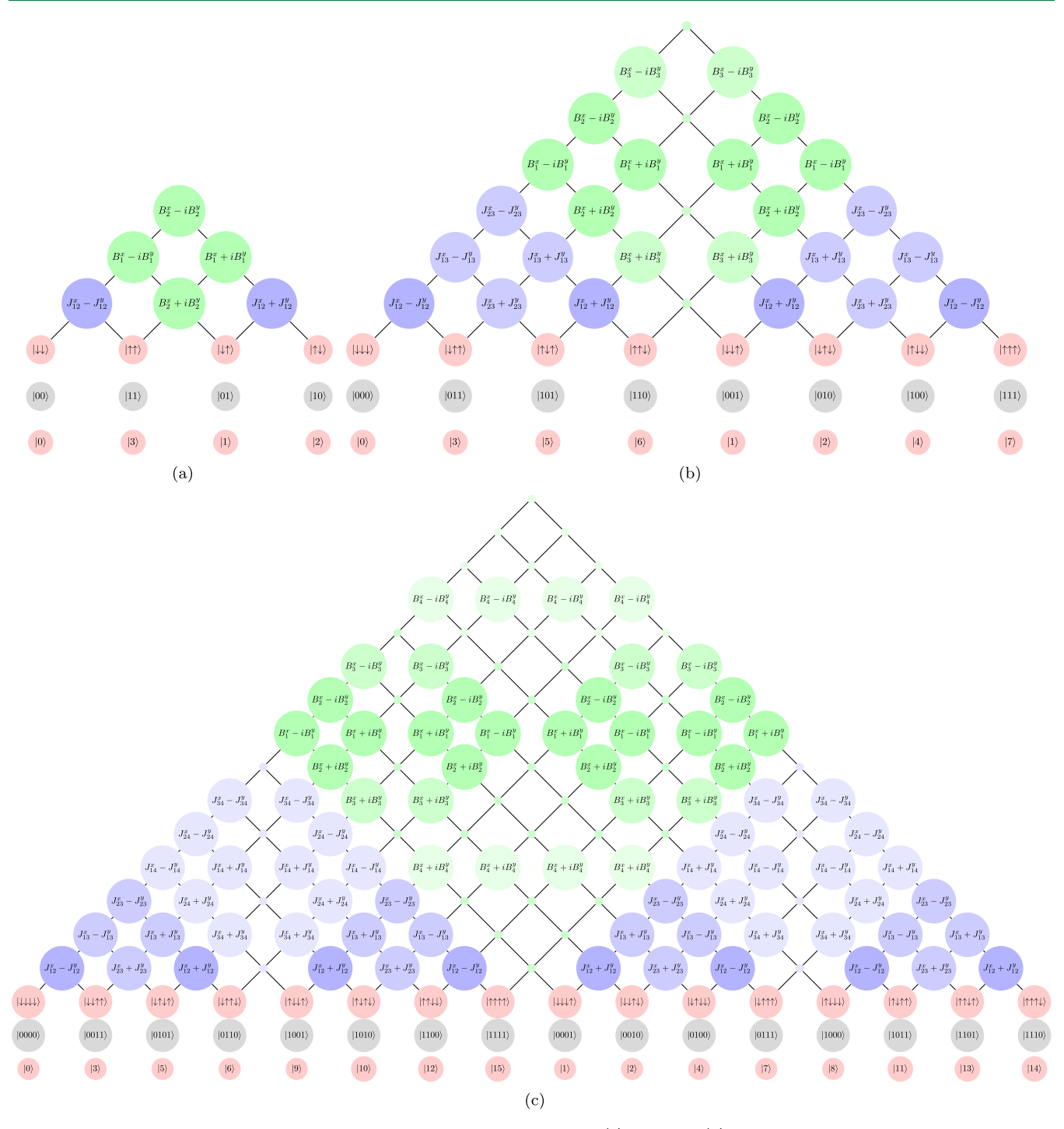


Figure 2. Recursive block structure of the Ising Hamiltonian in eq 1 for three (a) and four (b) qubits. The upper triangular portion of the Hamiltonian matrix is shown (excluding the diagonal). The computational basis is partitioned into odd,  $\{S^{+2n-1} \mid 00\cdots \}\}$ , and even,  $\{S^{+2n} \mid 00\cdots \}\}$ , spans of the total spin raising operators. The interaction between states  $|i\rangle$  and  $|j\rangle$  is the  $|j\rangle$  matrix element of the ion trap Hamiltonian. For example in (b),  $(0101)H_{TT}|1111\rangle = J_{13}^x - J_{13}^x$ . The off-diagonal blocks that couples the odd and even spans of the total spin-raising operators are marked in green. Zero coupling is represented by a "dot".

be manipulated to simulate a general form of the Ising-type Hamiltonian, as in eq 1, on a lattice of ions.

The Ising Hamiltonian structure exhibits inherent symmetries in terms of these control parameters that can be exploited to map a class of Hamiltonians to the quantum simulator. In ref 138, we show how a certain permutation of the computational basis in which such Hamiltonians are conventionally represented, reveals a block structure of the Hamiltonian. In this article, we provide a geometric

interpretation for the computational basis set ordering scheme through a generalized representation of the Bloch sphere. Through this geometric representation, we illustrate the classification of the computational basis that exposes the inherent symmetries present in the Ising Hamiltonian. Consequently, we discuss and illustrate the structure of the Ising Hamiltonian in this ordered basis set.

Conventionally, the spin-lattice Hamiltonian is represented in the  $2^N$ -dimensional space of spin-1/2 states where each spin

state corresponds to a two-level system that can be either up or down and equivalently  $|0\rangle$  or  $|1\rangle$ . A Bloch sphere (Figure 1a) provides a geometric representation of all pure states of a single-spin system. To generalize the Bloch sphere representation for a single spin to a higher number of spins, we borrow the idea of q-sphere from IBM Qiskit,  $^{166}$  to geometrically represent all  $2^N$  spin states of an N-qubit system. Figure 1 complements our discussion.

The q-sphere for an N-qubit system ( $N \ge 2$ ) is divided into rungs as follows. We begin by placing the all-down state 100··· 0) at the bottom pole or the  $0^{th}$  rung of the q-sphere. We then apply the total spin raising operator to this state, one spin at a time to obtain all other states in the higher rungs of the sphere. The action of the total spin raising operator once on the 0<sup>th</sup> rung yields all N-states that correspond to a single spin up and N-1 spins down. These are represented on a single plane close to the  $|00\cdots 0\rangle$ . See Figure 1. The action of the total spinraising operator on all states of this rung yields all possible N(N-1)/2 states of the 2<sup>nd</sup> rung, and these states are represented on the next plane. As we go to higher qubits, all possible  ${}^{N}C_{n}$  states for the  $n^{th}$  rung are obtained. This way, all basis states in the spin-lattice system are represented on the qsphere and the number of states in each rung of the q-sphere are identical to those encountered in Pascal's triangle. All combinations of spin states with the same total  $S_z$ -value occupy the same rung.

The geometrical representation of the N-qubit basis states using the q-sphere representation lends itself naturally to the classification of basis states we discuss for representing the Ising Hamiltonian. In ref 138, we note that the basis vectors created from acting an even number of lattice-site spin raising operators,  $\{S_i^+\}$  on the full down spin state,  $|00\cdots\rangle$ , yield the set,  $\{|00\cdots\rangle; S_i^+ S_i^+ |00\cdots\rangle; S_i^+ S_i^+ S_i^+ |00\cdots\rangle; \cdots\}, \text{ that are grouped }$ as part of one block of the ion-trap Hamiltonian and those that are obtained using an odd number of raising operators:  $\{S_i^+ \mid$  $00\cdots$ ;  $S_i^+ S_i^+ S_k^+ |00\cdots\rangle$ ;...} are grouped into a second block. The states belonging to the same block are represented using the same color (blue or red) in Figure 1. As can be seen in the qsphere representation in Figure 1, the action of the odd and even number of site-specific spin-raising operators on the alldown spin state |00..00\ranger corresponds to its alternating rungs. The alternating rungs can now be grouped to form the two basis set blocks in which the Ising Hamiltonian has a block structure, as discussed below and shown in Figure 2.

The diagonal elements of the Ising Hamiltonian, when represented in the computational basis, are linear combinations of all  $\{J_{ij}^z, B_i^z\}$  parameters. Figure 2 does not show these to maintain clarity. Since, inside each block of the permuted computational basis, the bases differ by at least two spin flips, the bases inside each block are connected by spin–spin coupling parameters  $\{J_{ij}^x, J_{ij}^y\}$  (shown in shades of purple in Figure 2a–c). Between the two blocks, the pairs of bases that differ by a single-spin flip or an odd number of flips are coupled by the  $\{B_i^x, B_j^y\}$  parameters, and hence those form the elements of the off-diagonal blocks of the Ising Hamiltonian in this permuted basis (as shown in green shades in Figure 2a–c). The structure derived here is completely general for N qubits, as can be seen in Figure 2a–c for two, three, and four qubits, respectively.

Furthermore, the diagonal and off-diagonal blocks for the N-qubit Ising Hamiltonian can be recursively obtained from those of the N-1 qubit Hamiltonian. This recursive structure within each block of the Ising Hamiltonian is illustrated in

Figure 2a-c using a gradient in colors, purple for the diagonal blocks with  $J_{ij}^x \pm J_{ij}^y$  elements and green for the off-diagonal blocks with  $B_i^x \pm iB_i^y$  matrix elements. For example, the recursion can be seen as follows for the diagonal block containing elements with spin-spin interaction terms. We begin with the elements of the diagonal block for a two-qubit Ising Hamiltonian as in Figure 2a,  $J_{ii}^x \pm J_{ii}^y$  for i = 1, and j = 2corresponding to the only spin-spin interaction in a two-qubit system shaded the darkest in all Figure 2a-c. The introduction of a third qubit introduces all possible spin-spin interactions  $J_{i3}^{x} \pm J_{i3}^{y}$  for all  $i \le 2$  as shown with the next shade of purple in Figure 2b. Similarly, all possible spin–spin interactions  $J_{i4}^x \pm J_{i4}^y$ for  $i \le 3$  also appear in the diagonal blocks of the 4-qubit Ising Hamiltonian as shown using the lightest shade of purple in Figure 2c. The 2- and 3-qubit diagonal block elements are nested in the 4-qubit Ising Hamiltonian. Therefore, with each additional qubit, the structure of the N-1 qubit Ising Hamiltonian is preserved, and blocks containing  $J_{iN}^x \pm J_{iN}^y$  for all  $i \le N - 1$ , the interaction of the  $N^{\text{th}}$  spin with the N - 1 spins are added. The off-diagonal blocks also have a similar recursive structure, wherein, with the addition of a qubit, a block with elements  $B_N^x \pm iB_N^y$  is added to the Ising Hamiltonian. This is made clear in Figure 2a-c with the gradation in green used for  $B_1^x \pm iB_1^y$ ,  $B_2^x \pm iB_2^y$ , and  $B_N^x \pm iB_N^y$  elements in the Hamiltonians. This block form of the Ising-type Hamiltonian and the associated structure in Figure 2, is a significant general result.<sup>138</sup> To the best of our knowledge, such a structure of the general Ising model was first discussed in ref 138, and we see that this analysis is critical for mapping arbitrary problems.

B. Nuclear Hamiltonian: Transformations That Yield a Block Diagonal Structure. The nuclear Hamiltonian is computed by using a coordinate representation, where the dimension along the donor—acceptor axis is discretized into  $2^N$  points. The matrix elements of the nuclear Hamiltonian,  $\mathcal{H}_{Mol}$  in this coordinate representation,  $\{|x_i\rangle\}$  is therefore given by

$$\langle x|\mathcal{H}_{Mo}|x'\rangle = K(x, x') + V(x)\delta(x - x') \tag{2}$$

The potential energy for the quantum dimensions is computed using standard electronic structure methods for which further details for each system are provided in the results section. The nuclear kinetic energy in this grid representation is approximated using the analytic banded Toeplitz Distributed Approximating Functionals (DAFs). <sup>167,168</sup>

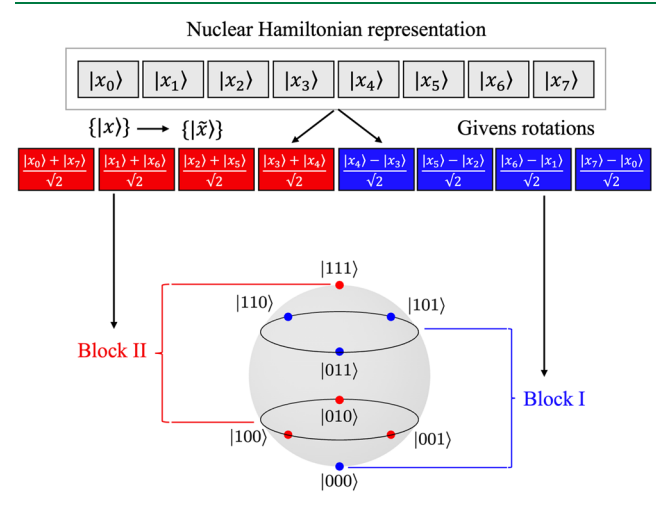
$$K(x, x') = K(|x - x'|) = \frac{-\hbar^2}{4m\sigma^3 \sqrt{2\pi}} \exp\left\{-\frac{(x - x')^2}{2\sigma^2}\right\}$$

$$\sum_{n=0}^{M_{DAF}/2} \left(\frac{-1}{4}\right)^n \frac{1}{n!} H_{2n+2} \left(\frac{x - x'}{\sqrt{2}\sigma}\right)$$
(3)

where  $H_{2n+2}\left(\frac{x-x'}{\sqrt{2}\sigma}\right)$  are the even order Hermite polynomials that only depend on the spread separating the grid basis vectors,  $|x\rangle$  and  $|x'\rangle$ , and  $M_{\mathrm{DAF}}$  and  $\sigma$  are parameters that together determine the accuracy and efficiency of the resultant approximate kinetic energy operator. The nuclear Hamiltonian,  $\mathcal{H}_{\mathrm{Mol}}$  in this coordinate representation,  $\{|x_i\rangle\}$ , therefore has a banded Toeplitz structure due to the structure of the kinetic energy when expressed in terms of DAFs. This banded Toeplitz representation of the DAF approximation for the kinetic energy operator in eq 3, where the property of its matrix elements,  $K_{ij} \equiv K(|i-j|)$ , has a critical role in reducing

the nuclear Hamiltonian to the form of  $\mathcal{H}_{IT}$  as discussed in ref 138 and summarized in Section II C.

The Householder and Givens transformations are commonly used matrix transformations that allow arbitrary matrices to be reduced to canonical forms. 169 Here, we use a sequence of Givens transformations to transform the banded Toeplitz form of the nuclear kinetic energy operator into a block diagonal form,  $\tilde{\mathcal{H}}_{Mol}$  that is commensurate with that of the Ising Hamiltonian in the permuted spin basis, as discussed in Section II. The details of the exact transformation are presented in section A of the Supporting Information (SI). Furthermore, this block diagonal form is maintained when the one-dimensional potential energy surface belongs to the C<sub>s</sub> point group, whose only symmetry operations are identity and reflection about a mirror plane. For cases where such symmetry does not exist, the more general set of transformations shown in Section III may be employed. The Givens matrix elements are the characters of this point group, and thus, with each Givens transformation, a rotation is effected in the two-dimensional plane of the pair of symmetrically located grid basis states. The resulting Givens transformed basis,  $\{|\widetilde{x_i}\rangle\}$ from the corresponding grid basis,  $\{|x_i\rangle\}$  is illustrated in Figure 3 for the case of eight grid points. We, therefore, exploit the



Ising Hamiltonian representation

Figure 3. Classification of the Givens transformed grid bases and the permuted computational bases in the q-sphere representation. Note that the Givens rotations result in symmetric and antisymmetric combinations of pairs of symmetrically located grid basis states. The map between the transformed Hamiltonians results from a map between the corresponding blocks of the basis of representation.

banded Toeplitz symmetry of the DAF kinetic energy operator and symmetry of the potential energy surface. The details of this transformation can be found in SI section A and ref 138, where the explicit transformations of each matrix element of the transformed Hamiltonian are given in terms of the elements of the banded Toeplitz Hamiltonian and the elements of the Givens matrices.

C. Obtaining Ion-Trap Parameters,  $\{B_i^z, J_{ij}^z\}$  from Transformed Nuclear Hamiltonian. As seen from the discussions in Sections II A and II B, the Ising Hamiltonian and the nuclear Hamiltonian both have block structures resulting from the permutation of the computational basis and the Givens transformation of the grid basis, respectively.

Owing to their commensurate structures, a direct map between each element of the nuclear Hamiltonian,  $\mathcal{H}_{\mathrm{Mol}}$  in the  $\{|\bar{x_i}\rangle\}$  basis to the corresponding elements of the Ising Hamiltonian,  $\mathcal{H}_{\mathrm{IT}}$  can be generated to compute the Ising Hamiltonian parameters. Our goal is to use the diagonal and off-diagonal elements of  $\tilde{\mathcal{H}}_{\mathrm{Mol}}$  to obtain the sets of ion-trap parameters  $\{B_i^z, J_{ij}^z\}$  and  $\{J_{ij}^x, J_{ij}^y\}$ , respectively. This establishes a map between the given transformed grid basis and the permuted computational basis, as shown in Figure 3. The mapping expression between the elements of the molecular Hamiltonian and the corresponding elements of the ion-trap Hamiltonian may be written as

$$\langle \tilde{\mathbf{x}} | \mathcal{H}_{\mathsf{Mol}} | \tilde{\mathbf{x}}' \rangle \equiv \langle \tilde{\lambda} | \mathcal{H}_{\mathsf{IT}} | \tilde{\lambda}' \rangle \tag{4}$$

for  $|\vec{\lambda}\rangle$  corresponding to the computational bases in blocks I or II for the Ising Hamiltonian (as discussed in Section II A and shown in Figures 1 and 3). Using eq 2 and the transformations discussed in Section II B (detailed in SI A) to write the elements of  $\tilde{\mathcal{H}}_{Mol}$  and the corresponding Ising Hamiltonian matrix elements for eq 1, for the left and right sides of eq 4 corresponding to the diagonal elements only, we obtain

$$\begin{split} & [K(x_i, x_i) - K(x_i, x_{n-i})] + \frac{1}{2} [V(x_i) + V(x_{n-i})] \\ & = \sum_{j=1}^{N} (-1)^{\tilde{\lambda}_j} B_j^z + \sum_{j=1}^{N-1} \sum_{k>j}^{N} (-1)^{\tilde{\lambda}_j \oplus \tilde{\lambda}_k} J_{jk}^z \\ & \text{for } i \le n/2 \end{split} \tag{5}$$

$$& [K(x_i, x_i) + K(x_i, x_{n-i})] + \frac{1}{2} [V(x_i) + V(x_{n-i})] \\ & = \sum_{j=1}^{N} (-1)^{\tilde{\lambda}_j} B_j^z + \sum_{j=1}^{N-1} \sum_{k>j}^{N} (-1)^{\tilde{\lambda}_j \oplus \tilde{\lambda}_k} J_{jk}^z \\ & \text{for } i > n/2 \end{aligned} \tag{6}$$

where  $\oplus$  on the right side denotes the addition modulo 2,  $\tilde{\lambda}_j$  is the  $j^{\text{th}}$  bit of the bit representation of  $|\tilde{\lambda}\rangle$  with values 0 or 1 as shown in Figures 1 and 2.

A detailed discussion on this map is provided in ref 138, where it is shown that the ion-trap control parameters,  $\{B_i^z; J_{ij}^z\}$  are specific Hadamard transforms of  $\langle \tilde{x}|\mathcal{H}_{\text{Mol}}|\tilde{x}\rangle$ . In a similar manner, the off-diagonal elements of  $\tilde{\mathcal{H}}_{\text{Mol}}$  are mapped to the corresponding  $\mathcal{H}_{\text{IT}}$  elements to obtain the  $\{J_{ij}^x; J_{ij}^y\}$  parameters. The map is approximate for a higher number of qubits, for which the error estimates are provided in ref 138. In Figure 4, the map is illustrated for the  $H_3O_2^-$  system to be studied later in the publication.

The reasons behind the intrinsically approximate nature of the mapping algrithm are discussed in detail in ref 138. We summarize the main features here. In essence, as the number of qubits N increases, the Ising Hamiltonian parameters (B and J handles in eq 1) scale as,

$${N + N(N-1)/2} + {N(N-1)} \rightarrow O(N^2)$$
 (7)

Here (a) the first quantity,  $\{N + N(N-1)/2\}$ , refers to the parameters,  $\{B_i^z; J_{ij}^z\}$ , that form the diagonal elements of the Ising matrix, (b) the second quantity on the left,  $\{N(N-1)\}$ , refers to the parameters,  $\{J_{ij}^x \pm J_{ij}^y\}$ , that control the off-diagonal elements. This scaling and structure of the spin-lattice

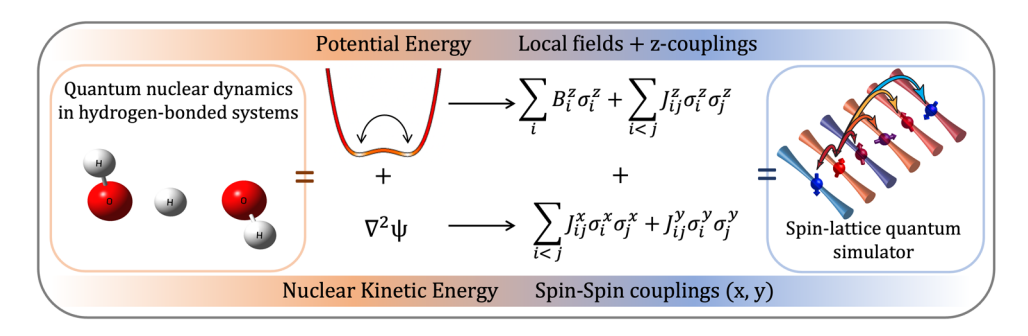


**Figure 4.** Outline of the mapping algorithm: The algorithm converts the Born–Oppenheimer potential surface and kinetic energy terms in a quantum nuclear problem to a set of controllable ion-trap parameters,  $\{\{B_i^z\}; \{J_{ij}^x, J_{ij}^y, \text{ and } J_{ij}^z\}\}$ , and facilitates the dynamical evolution of quantum states in an ion trap.

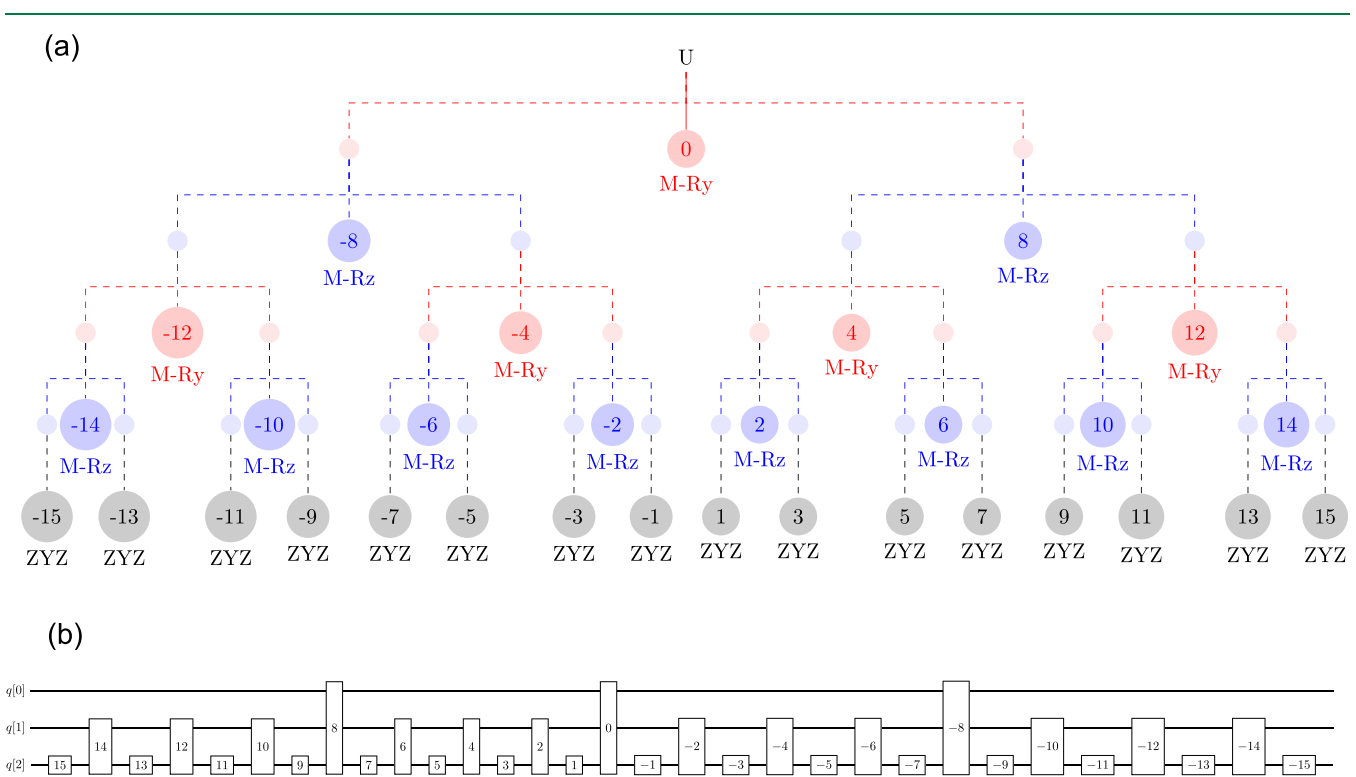


Figure 5. (a) Decomposition of a 3-qubit unitary, U, into one and two-qubit gates. The decomposition involves alternate layers of the CSD (red) and VDW (blue). M-Rz(Ry) are N and N-1 qubit multiplexed Rz(Ry) gates which can be further decomposed into a set of CNOT and Rz(Ry) gates. The ultimate layer (gray) involves decomposition into single-qubit gates. (b) Schematic of the circuit resulting from the Quantum Shannon decomposition in (a). All single-qubit operations (on q[2]) are decomposed using the ZYZ decomposition, while all multiqubit operations are either multicontrolled  $R_v$  or  $R_z$  operations as discussed in Section III.

Hamiltonian, <sup>138</sup> may restrict the mapping of a general unitary operator, since a general  $2^N \times 2^N$  unitary matrix may have  $O(2^N)$  independent elements. Thus, as the number of qubits increases, the mapping algorithm becomes more and more approximate as the number of equations given by eqs 5 and 6 exceeds the number of spin–lattice parameters  $\{B_i^{\gamma}; J_{ij}^{\gamma}\}$ . However, it may also be possible to reduce the number of actual parameters within the  $2^N \times 2^N$  unitary matrix and these aspects will be considered in future publications. <sup>140</sup>

## III. QUANTUM SHANNON DECOMPOSITION: REDUCTION OF ARBITRARY UNITARY OPERATIONS INTO QUANTUM CIRCUITS

The mapping protocol necessitates that the number of  $\{B_i^x, B_i^y, B_i^z\}$ , and  $\{J_{ij}^x, J_{ij}^y, J_{ij}^z\}$  parameters in the Ising Hamiltonian match the number of parameters in the molecular Hamiltonian. Since

we also consider a fine grid for our potential energy surface with an equivalent increase in the number of qubits, it is critical to note that the molecular Hamiltonian matrix size grows exponentially while the number of Ising Hamiltonian parameters only grows quadratically (see ref 138). Consequently, the map between the molecular Born-Oppenheimer Hamiltonian and the Ising Hamiltonian becomes more and more approximate as the number of qubits grows. To address this and achieve an accurate treatment of the chemical dynamics process for a larger number of qubits, we introduce a quantum circuit decomposition method here. The unitary propagator corresponding to the molecular Hamiltonian is written as a quantum circuit, which is then used to simulate the temporal evolution of the molecular system. It has been shown that an arbitrary unitary matrix can be decomposed into a universal quantum gate set consisting of a few single-qubit gates along with a two-qubit entangling gate. 170 Several matrix decomposition techniques such as the QR, Givens, Householder, and cosine-sine decomposition have been used to obtain quantum circuits for arbitrary unitary operators 170,171 resulting in universal quantum gate sets. In this section, we adapt the Quantum Shannon decomposition (QSD)<sup>143</sup> for the quantum circuit decomposition of unitary matrices obtained in quantum chemical dynamics processes. The decomposed unitaries are equivalent to unitary gate operations that can be implemented using standard quantum gates from a universal gate set on quantum hardware. This allows execution of an arbitrary unitary operation as a concatenated sequence of universal gates on a given quantum hardware. The decomposition scheme involves two well-known matrix decomposition schemes—the cosine-sine decomposition (CSD)<sup>172-174</sup> and the joint eigenvalue-based decomposition of block diagonal unitaries referred to here as VDW<sup>171</sup> scheme. A brief description of the algorithm is provided below. One key outcome from the algorithm below is that the number of entangling gates in this algorithm can be estimated at  $\frac{3}{4}4^n - \frac{3}{2}2^n$  which is close to the theoretical lower bounds to the number of CNOT gates,  $\frac{1}{4}(4^n - 3n - 1)$ , as discussed in

We begin by considering a  $2^N$  by  $2^N$  unitary matrix that is to be implemented on a quantum computer by using universal gates. We consider the universal gate set  $\{R_y(\theta), R_z(\theta), \text{CNOT}\}$ , consisting of single-qubit rotation operations,  $R_y(\theta)$  and  $R_z(\theta)$  that affect rotations about the y and z axis of the Bloch sphere by arbitrary angles  $\theta$ , and the two-qubit operation, CNOT. A flow of the decomposition is provided as a tree diagram in Figure 5a. The CSD (shown in red in Figure 5a) and VDW (shown in blue in Figure 5a) steps iteratively break down the  $2^N$  by  $2^N$  unitarily to a sequence of these single- and two-qubit operations. The CSD decomposes the unitary matrix, U, into a product of three unitaries with distinct structures,

$$U = \begin{pmatrix} \mathbf{L}_0 & \mathbf{0} \\ \mathbf{0} & \mathbf{L}_1 \end{pmatrix} \begin{pmatrix} \mathbf{C} & -\mathbf{S} \\ \mathbf{S} & \mathbf{C} \end{pmatrix} \begin{pmatrix} \mathbf{R}_0 & \mathbf{0} \\ \mathbf{0} & \mathbf{R}_1 \end{pmatrix}$$
(8)

where the left(L) and right(R) matrices are block diagonal unitaries with blocks  $L_0$ ,  $L_1$  and  $R_0$ ,  $R_1$ , respectively. C and S are diagonal matrices with entries  $\cos(\alpha_i)$  and  $\sin(\alpha_i)$ , respectively, for  $i = 0 - 2^{N-1}$ . This cosine—sine (CS) matrix (node 0 in Figure 5a) is a multiple-control  $R_v$  gate. A multicontrol <sup>143</sup> gate can be cast as an N-qubit generalization of a conditional gate in a quantum circuit, wherein each of the  $2^{N-1}$  conditions implemented using N-1 control qubits results in a different unitary operation on the N<sup>th</sup> target qubit. These may be referred to as  $CCC \cdots R_{\nu}$  operations. A multicontrol  $R_{\nu}$  can, therefore, be thought of as a conditional operation of a  $\hat{R}_{\nu}(\alpha_i)$  rotation on the target qubit depending on the  $i^{th}$  condition enforced by N-1 qubits. This simultaneous operation of the  $2^{N-1}$   $R_{\nu}(\alpha_i)$ 's for all values in  $\{\alpha_i\}$  can be decomposed further and implemented using  $2^{N-1}$  CNOT's and  $2^{N-1} R_{\nu}(\theta_i)$  rotation gates. The rotation angles  $\theta_i$  can be obtained from linear combinations of  $\alpha$ 's using a Gray code method as outlined in ref 175. Classically, one can think about this as  $2^{N-1}$  conditionality statements, one condition representing a specific  $R_{\nu}$  rotation; only, on a quantum computer these are meant to be executed in parallel. While such operations may in principle represent the true power of

quantum devices in the future, in the NISQ era, <sup>176,177</sup> these operations are deeply limited by the number of CNOT gates required to implement them.

The block diagonal unitaries on the left and right in eq 8 (red empty nodes in Figure 5a), are N-qubit conditional gates, known as quantum multiplexors, with a single-qubit control and corresponding conditional operation on N-1 target qubits. At this point, it is important to reiterate and note the difference in the structures of the block diagonal L, R matrices and the CS matrix and the resulting multiqubit gates. While the N-qubit operation corresponding to the CS unitary matrix, as discussed earlier, has multiple controls (precisely  $2^{N-1}$  for an N-qubit unitary), and a single-target qubit, that for the L, R matrices have a single control with N-1 target qubits. This decomposition technique thus exploits these two generalizations to multiqubit gates to build the entire quantum circuit corresponding to U. The VDW transformation, as given by eq 9, is a technique for decomposing such quantum multiplexor gates (obtained from the L and R matrices above), with a single-control and multiple-target qubits, into basic quantum circuit unitaries. The L and R matrices from eq 8 are thus further decomposed into,

$$L = \begin{pmatrix} \mathbf{L}_0 & \mathbf{0} \\ \mathbf{0} & \mathbf{L}_1 \end{pmatrix} = \begin{pmatrix} \mathbf{V} & \mathbf{0} \\ \mathbf{0} & \mathbf{V} \end{pmatrix} \begin{pmatrix} \mathbf{D} & \mathbf{0} \\ \mathbf{0} & \mathbf{D}^{\dagger} \end{pmatrix} \begin{pmatrix} \mathbf{W} & \mathbf{0} \\ \mathbf{0} & \mathbf{W} \end{pmatrix}$$
(9)

The VDW is critical in that left and right block diagonal matrices containing V and W, respectively, correspond to N – 1 qubit operations in a quantum circuit. Therefore, each VDW step in the decomposition halves the dimension of the unitary matrix. This step is shown in blue in Figure 5a and the V and W matrices are blue nodes in Figure 5a. The V and W matrices are further decomposed by using CSD in the next step. The diagonal matrix, D, (node -8 for L and 8 for R in Figure 5a) is a multicontrol  $R_z$  gate (similar to the multicontrol  $R_v$  operation for the CS matrix) and can be decomposed further into a sequence of  $2^{N-1}$  CNOT's and  $2^{N-1}$   $R_z(\theta)$  gates, similar to the decomposition of the cosine-sine matrix as a multiplexed  $R_{\nu}(\theta)$ . As noted above, these multiplexed  $R_{z}(\theta)$  operations are also akin, now, to  $2^{N-2}$  conditionality statements. Following N - 1 steps of alternating CSD and VDW steps, the resultant matrices are single-qubit units, which are further decomposed using the ZYZ scheme for arbitrary single-qubit unitaries. The multiplexors are decomposed into single-qubit rotation gates and CNOT gates using a gray code implementation as outlined in ref 175. Thus, the QSD yields a quantum circuit of multicontrolled  $R_v(\theta)$  and  $R_z(\theta)$  gates, and single-qubit unitaries, which have standard procedures to be further decomposed into the gates in the universal gate set  $\{R_{v}, R_{z}, R_{$ CNOT}. The numbered nodes of Figure 5a correspond to these multicontrolled and single-qubit unitaries, and for clarity, the circuit schematic corresponding to the decomposition is provided in Figure 5b. Note that the order is reversed in the quantum circuit for showing the action of *U* on an initial qubit state.

The number of gates in any standard implementation of this decomposition is estimated from the implementation of the multicontrolled  $R_y(\theta)$  and  $R_z(\theta)$  gates. This scheme has the advantage that when a fixed gate set is used to construct the circuit, the resulting circuits have a constant circuit depth for an arbitrary  $2^N$  by  $2^N$  dimensional unitary. This implementation assumes the use of the universal gate set  $\{R_y, R_z, CNOT\}$  as is apparent from the summary above, but is not limited by

this gate set alone. Each  $2^N$  by  $2^N$  multiplexed- $R_y(R_z)$  requires  $2^{N-1}$  CNOTs and  $2^{N-1}$   $R_y(R_z)$  gates using the gray code implementation as discussed in ref 143. There is an inherent structure in the decomposition scheme that is evident from the decomposition of general multiplexed  $R_y$  and  $R_z$  gates as shown in ref 143. This structure of the decomposition is irrespective of the inherent symmetries present in the unitary itself.

# IV. PROTON STRETCH DYNAMICS IN $\rm H_5O_2^+$ AND $\rm H_3O_2^-$ USING THE MAPPING PROTOCOL AND USING QUANTUM SHANNON DECOMPOSITION

We examine the map in Section II and the quantum circuit decomposition method in Section III by simulating and comparing the quantum dynamics of the shared proton in the protonated Zundel ( $H_5O_2^+$ ) and the corresponding hydroxide water clusters  $(H_3O_2^-)$ . In examining the mapping protocol, we simulate and compare the dynamics of both the molecular systems and their corresponding ion-trap dynamics on classical hardware, independently. The Ising model Hamiltonian that we consider for validating the mapping protocol is for a trapped ion system with three qubits. In simulating the proton transfer dynamics for each of the systems, we study the time evolution of the initial nuclear wavepacket states prepared in the respective permuted basis representations for the molecular and Ising model Hamiltonians. As stated, the parameters in the Ising Hamiltonian are determined, and thus controlled, by the precomputed matrix elements of the molecular Hamiltonian. In implementing the circuit decomposition technique, we simulate the unitary time evolution of the transferring proton in the water clusters by decomposing the unitary propagator,  $e^{-iHt/\hbar}$ , for each value of t into a sequence of quantum gates using the Quantum Shannon decomposition method detailed in Section III. We implement the resulting quantum circuits on IBM's QASM simulator using their software development kit, Qiskit. In the following sections, we first introduce the molecular systems that we consider to validate our mapping protocol and circuit decomposition scheme. In Section IV A, we outline the computational details of the potential energy surfaces and the quantum nuclear Hamiltonian, followed by the time evolution of the quantum nuclear wavepacket, for both the systems under consideration in Sections IV B and IV C.

Water clusters are an important class of molecular systems found in many constrained environments such as biological membranes, enzyme active sites, \$^{178,179}\$ and ion channels.\$^{180}\$ Water-mediated "proton wires," for example, are routinely invoked to explain charge transport across cell membranes and the primary charge-separation step in photosynthesis. They may also be confined within carbon nanotubes leading close to ballistic transport, \$^{181-183}\$ and are a critical aspect of polymer electrolyte fuel cells. \$^{184}\$ The lighter mass of the hydrogen nucleus makes quantum nuclear effects critical in all such cases; \$^{185-188}\$ additionally, the multidimensional quantum nuclear effects in such systems arising from the vibrational coupling between the proton transfer dimensions and other orthogonal modes are also known to be critical in such problems.  $^{1,53,58,61}$ 

The chemical systems considered in this article are specific small protonated and hydroxide-rich water clusters. The isolated  $H_5O_2^+$  and  $H_3O_2^-$  ions are two of the most fundamental structures involved in the proton transfer process. The anionic  $H_3O_2^-$  complex is especially interesting because it involves a strong low-barrier hydrogen bond (LBHB),  $^{7-9,148,149}$  a

phenomenon often introduced to explain the surprisingly high rates of some enzyme-catalyzed reactions. 145,146,189,190 Based on the studies of small molecules, such short, strong HBs are often formed between functional groups with comparable  $pK_a$ 's and often result in a zero point energy for the shared hydrogen higher than the barrier height energy for proton transfer. The Zundel cation is a small prototypical system with a proton shared between two water molecules forming a short, strong hydrogen bond. 53,58-61,76,137 This system plays a fundamental role in the understanding of processes such as the enhanced mobility of protons and deuterons in condensed phase aqueous environments, in biological systems, and several problems of interest in materials chemistry, such as protonic conductors and fuel cells. 150-153 Due to their central role in aqueous charge transport, the  $H_5O_2^+$ and H<sub>3</sub>O<sub>2</sub><sup>-</sup> ions have been extensively investigated with electronic structure theory and quantum nuclear dynamics, 58-60 and both display stable configurations where one hydrogen atom resides between the two oxygen atoms (e.g.,  $[H_2O\cdots H\cdots OH_2]^+$  and  $[HO\cdots H\cdots OH]^-$ ).

A. Computation of the Nuclear Hamiltonians Describing Proton Transfers in  $H_3O_2^-$  and Zundel Clusters. We compute one-dimensional potential energy surfaces for the intramolecular proton transfer mode in both  $H_3O_2^-$  and  $H_5O_2^+$ , by first locating a stationary point for both systems where the proton is symmetrically shared between the donor and acceptor groups. For the case of H<sub>2</sub>O<sub>2</sub>, this corresponds to the transition state, with one imaginary frequency of the Hessian matrix corresponding to the vibrational mode along the intramolecular proton transfer direction. For the case of the protonated Zundel, however, the geometry in which the donor and acceptor atoms symmetrically share the proton corresponds to a minimum. Standard electronic structure methods are employed to perform these computations. Born-Oppenheimer potential energy surfaces for one-dimensional proton motion along the donor-acceptor axis are computed for these stationary point geometries. For that purpose, we choose a one-dimensional grid along the donor-acceptor axis with 2<sup>N</sup> number of equally spaced grid points, symmetrically located about the stationary point (grid center). We perform electronic structure calculations at these points, on a classical computing platform, at the level of theory mentioned in Table I for the range N = 3 to N = 7. Details of the electronic structure methods and total grid lengths for these potential energy surface calculations are listed in Table I.

B. Quantum Simulation of Proton Transfer Dynamics in  $H_3O_2^-$  and Zundel Using the Mapping Protocol. We

Table I. Computational Details for Computing the Potential Energy Surfaces for the Transferring Proton in Both Water Clusters  $^a$ 

system	DA-distance (Å)	level of theory	grid spread (Å)	no. of grid points
$H_{3}O_{2}^{-}$	2.42	CCSD/6-311+ +G(d,p)	0.66	8,16,32,64,128
$H_5O_2^+$	2.39	B3LYP/6-311+ +G(d,p)	0.66	8,16,32,64,128

<sup>a</sup>In all cases, the grid spacing ranges from 0.083 Å (for 8 grid points, that is three qubits) to 0.005 Å (for 128 grid points, that is 7 qubits). The finer grid spacings essentially approach the continuous limit, given the mass of the proton and associated de Broglie wavelength. Also see Figure 6 for associated smoothness of potential.

Table II. Parameters and Characteristics of the Initial Wavepacket States Considered for Transferring the Proton in the Water Cluster Systems<sup>a</sup>

		$\mathrm{H_{3}O_{2}^{-}}$			$H_5O_2^+$		
initial wavepacket	parameters	$ \langle \chi_0   \psi \rangle ^2 $ (%)	$E^{b}$	$\epsilon^c$	$ \langle \chi_0   \psi \rangle ^2 $ (%)	$E^{\boldsymbol{b}}$	$\epsilon^c$
$\psi_L(x; 0) = \delta (x - x_0)$	$x_0 = donor site$	0.27	28.1	$10^{-15}$	0.08	35.1	$10^{-7}$
$\psi_G(x; 0) = \exp\left[-\frac{(x-\mu)^2}{2\sigma^2}\right]$	$\sigma=0.1$ Å, $\mu=0.0$ Å	87.7	2.41	$10^{-15}$	93.71	2.6	$10^{-7}$
$\psi_T(x; 0) = \sum_j \exp[-E_j/kT]\chi_j(x)$	T = 300  K	99	1.34	$10^{-15}$	99.92	1.92	$10^{-7}$

<sup>a</sup>The ground state,  $|\chi_0\rangle$ , overlap for each  $|\psi(x;0)\rangle$  and corresponding energy are reported for the case of N=3. The mean absolute errors in probability,  $\epsilon$ , computed between the classical propagated probability density,  $\rho_C(x)$ , and the probability density,  $\rho_Q(x)$ , computed using the mapping protocol in Section II, are provided. <sup>b</sup>In units of kcal/mol. <sup>c</sup>As in eq 10.

examine the map by simulating the quantum dynamics of the water clusters and the ion-trap dynamics on classical hardware, independently. For that, we choose the initial wavepacket state for the transferring proton in both systems in three different ways in the grid representation (x), the details of which are provided in Table II. The three initial wavepackets considered here are designed to probe a broad range of energy. The wavepacket  $\psi_L(x; 0)$  is particularly harsh given that it samples almost the full eigenspectrum, whereas the other two choices populate the lower regions of the energy spectrum. The corresponding Givens transformed wavepacket initial state is considered for time evolution using the block diagonal molecular Hamiltonian in the mapping protocol. Given the direct map described in Section II C between the permuted computational basis and the Givens transformed molecular grid basis, the initial wavepackets for the Ising Hamiltonian are chosen analogously to the initial wavepacket of the molecular system. The wavepacket state,  $\psi_L(x; 0)$ , initialized on the end of the grid close to the donor site (as in Table II), corresponds  $\left\{\frac{|\tilde{x}_0\rangle - |\tilde{x}_7\rangle}{\sqrt{2}}\right\}$  in the Givens transformed basis. The corresponding initial state for the Ising Hamiltonian is chosen analogously to be  $\left\{\frac{|\tilde{\lambda_0}\rangle - |\tilde{\lambda_7}\rangle}{\sqrt{2}}\right\}$  in the permuted computational basis,  $\{|\tilde{\lambda}\rangle\}$ .  $\psi_G(x; 0)$  and  $\psi_T(x; 0)$  are symmetric about the center of the grid and are mostly concentrated on the first block of the Givens transformed basis. The spin-lattice and molecular wavepackets are then independently propagated according to the transformed Ising and molecular Hamiltonians and compared to gauge the accuracy of the quantum simulation.

Given the map between the matrix representation of the Ising Hamiltonian and the Givens transformed molecular Hamiltonian (in eq 4), as discussed in ref 138, the ion-trap hardware initial wavepacket state is directly propagated by the choice of  $\{B_i^{\gamma}; J_{ij}^{\gamma}\}$  for arbitrary time-segments. The time-dependent probabilities resulting from the projection of the resultant time-dependent wavepacket on the computational basis, at each interval of time, are used to compute the difference between the classical and quantum algorithms:

$$\epsilon = \frac{1}{T} \int dt \frac{1}{2^N} \int dx |\rho_Q(x) - \rho_C(x)| \tag{10}$$

where  $\rho_Q(x)$  and  $\rho_C(x)$  are the quantum and classical values of the wavepacket density, respectively, N is the number of qubits (ions), and T is the total simulation time. The resultant errors are listed in Table II.

Given the exact match between the spin-lattice dynamics and the quantum chemical dynamics, the features present in

ion-trap dynamics must also exist in the chemical dynamics problem. Thus, through the isomorphism constructed above, our algorithm allows the ability to extract properties of the chemical systems from the corresponding Ising Hamiltonian dynamics on the ion trap.

C. Quantum Simulation of Proton Transfer Dynamics in  $H_3O_2^-$  and Zundel Using Quantum Shannon Decomposition. The proton dynamics in the water clusters as simulated using the mapping protocol is exact for the case of N = 3. However, the number of grid points in that case does not capture the important characteristics of the potential energy surface, as is clear from Figure 6. We therefore simulate the

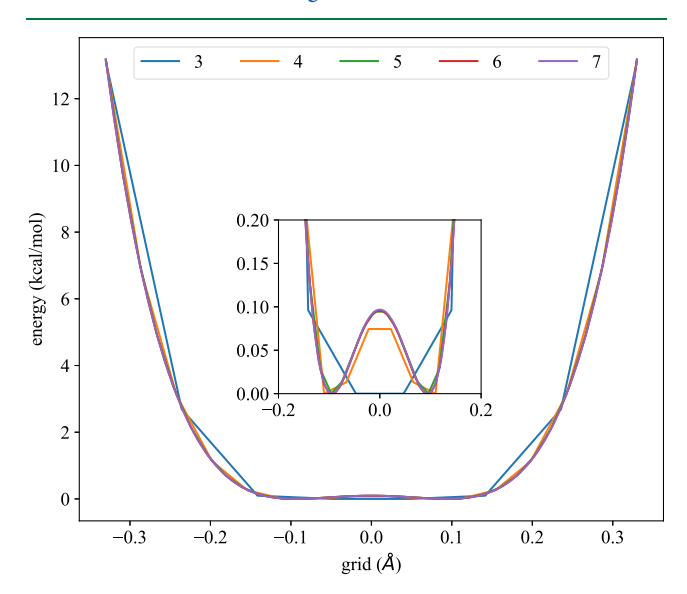


**Figure 6.** One-dimensional potential energy surfaces for the proton along the donor—acceptor axis in  $H_3O_2^-$  computed using a range of grid separations (refer Table I). The surfaces converge with increasing gridpoint densities (64 and 128 for N=6 and N=7, respectively). The low barrier height is shown in the inset for all gridpoint densities.

circuit decomposed unitary evolution of the proton wavepacket for more accurate representations of the chemical problem for N=3 to 7 qubits. The unitary propagator,  $e^{-i\hat{H}t/\hbar}$ , for each value of t are decomposed into a sequence of quantum gates using the Quantum Shannon decomposition method detailed in Section III. This decomposition will result in a significantly lower number of gates since the number of gates remains constant compared to a Trotter-based decomposition where the circuit depth and gate counts double with subsequent Trotter steps. We implement the resulting quantum circuits on IBM's QASM simulator using their software development kit, Qiskit. Probability densities are measured after unitary

Table III. Mean Absolute Errors in Probability (eq 10) Computed between the Classical Propagated Probability Density  $\rho_C(x)$  and the QASM Simulated Probability Densities,  $\rho_O(x)$ , Using the Circuit Decomposition Method Summarized in Section III<sup>a</sup>

	$\epsilon$ (eq 10) for ${ m H_5O_2^+}$				$\epsilon$ (eq 10) for ${ m H_3O_2^-}$					
initial wavepacket	N = 3	N = 4	N = 5	N = 6	N = 7	N = 3	N = 4	N = 5	N = 6	N = 7
$\psi_L(x; 0)$	$6 \times 10^{-4}$	$5 \times 10^{-4}$	$4 \times 10^{-4}$	$3 \times 10^{-4}$	$2 \times 10^{-4}$	$7 \times 10^{-4}$	$5 \times 10^{-4}$	$4 \times 10^{-4}$	$3 \times 10^{-4}$	$2 \times 10^{-4}$
$\psi_G(x; 0)$	$6 \times 10^{-4}$	$5 \times 10^{-4}$	$4 \times 10^{-4}$	$3 \times 10^{-4}$	$2 \times 10^{-4}$	$7 \times 10^{-4}$	$5 \times 10^{-4}$	$4 \times 10^{-4}$	$3 \times 10^{-4}$	$2 \times 10^{-4}$
$\psi_T(x; 0)$	$6 \times 10^{-4}$	$5 \times 10^{-4}$	$4 \times 10^{-4}$	$3 \times 10^{-4}$	$2 \times 10^{-4}$	$7 \times 10^{-4}$	$5 \times 10^{-4}$	$4 \times 10^{-4}$	$3 \times 10^{-4}$	$2 \times 10^{-4}$

<sup>a</sup>The number of shots is 1000. Errors are reported for different initial nuclear wavepacket states of the transferring proton in both water clusters for all cases of N = 3 - 7. As the number of shots is increased, the error decreases, as noted in Figure 7.

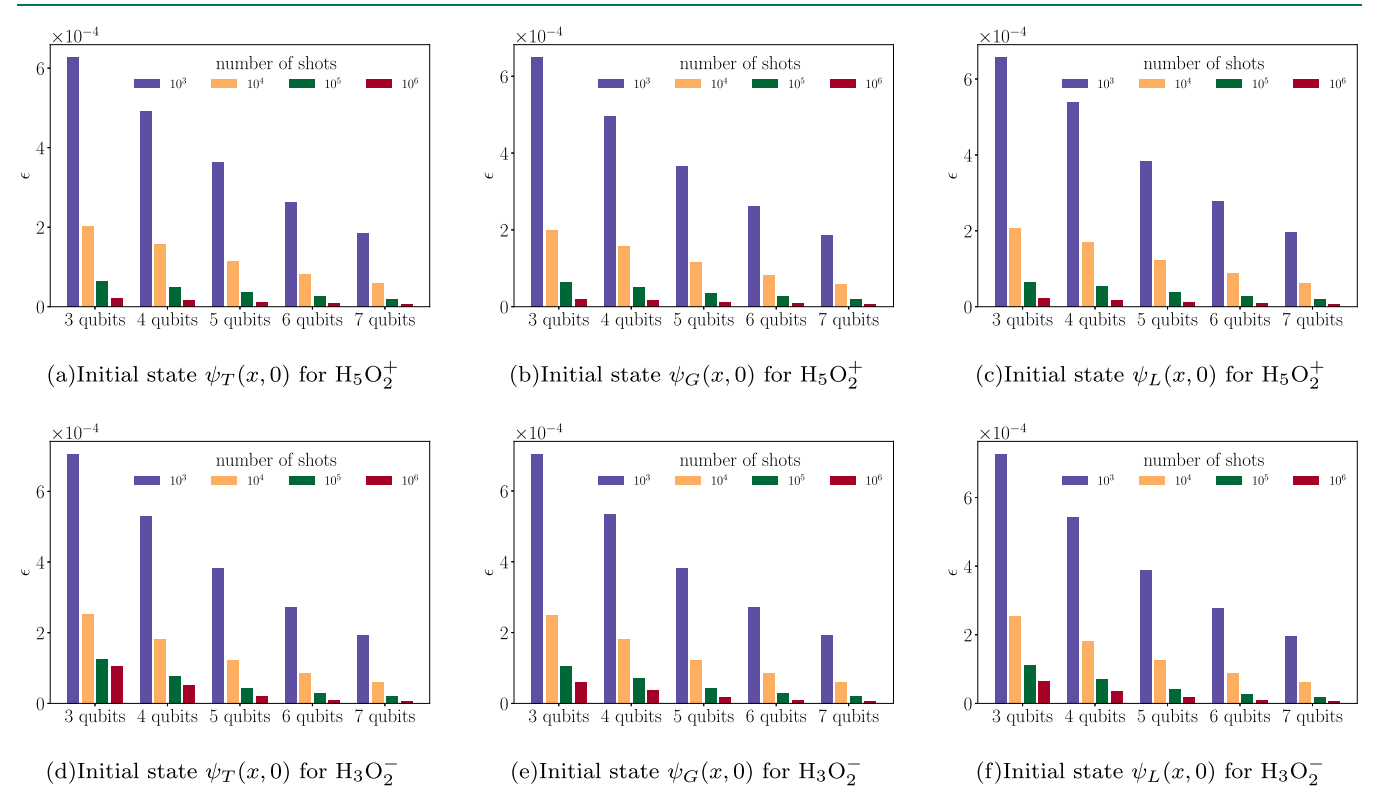


**Figure 7.** Vertical axes show probability errors, ( $\epsilon$  in eq 10) for N = 3 - 7 qubits and for the different initial nuclear wavepacket states as a function of the number of measurement shots on IBM's QASM simulator for both chemical systems. Clearly the error reduces drastically with increasing shots.

evolution at each time step. The errors in probability densities for the circuit implementation and classical propagation are computed using eq 10 and reported in Table III for the proton transfer dynamics in the protonated and hydroxide water clusters. Since the QASM simulator emulates the behavior of an actual quantum device, in the absence of a noise model, the precision of the estimated probabilities depends entirely on the number of measurement shots used for each time step. For about 1000 shots per time step, the error in the probabilities is on the order of  $10^{-4}$ , across all qubit cases, as reported in Table III. We also report probability errors for an increasing number of measurement shots and see agreement of up to 10<sup>-6</sup>. Figure 7 shows how the error improves as we increase the number of shots from 10<sup>3</sup> to 10<sup>6</sup> for all qubit cases and appears to indicate the accuracy of our QSD transformation algorithm. Furthermore, we compute the Fourier transform of the measured time-evolved probability densities,  $\rho_{O}(x, t)$ , which results in a spectrum with Fourier peaks corresponding to the frequency differences among the energy eigenvalues. The relevant details are provided in SI Section IV. We can extract the oscillation frequencies of the shared proton in both chemical systems

from these Fourier spectra of the frequency differences. In Figure 8, we compare the lower-level eigenenergies obtained from the Fourier transform of the time-evolved probabilities on QASM to those obtained from the corresponding exact diagonalization for all bound eigenstates for both chemical systems for qubit cases N = 3 - 7. The absolute errors between the QASM simulated eigenenergies and the exact diagonalization results are well below 1 kcal/mol for the lower energy levels for  $H_5O_2^+$  and  $H_3O_2^-$ .

#### V. CONCLUSIONS

The promise of solving exponentially complex problems efficiently using quantum computing hardware and associated quantum computing algorithms software is a rapidly evolving research frontier. While we are in the early stages of this quantum revolution, there is a wide set of scientific and technological areas that can benefit from such developments. However, true progress in such areas can only be achieved by a rigorous study and understanding of the electronic structure and dynamics of complex materials, thus requiring accurate

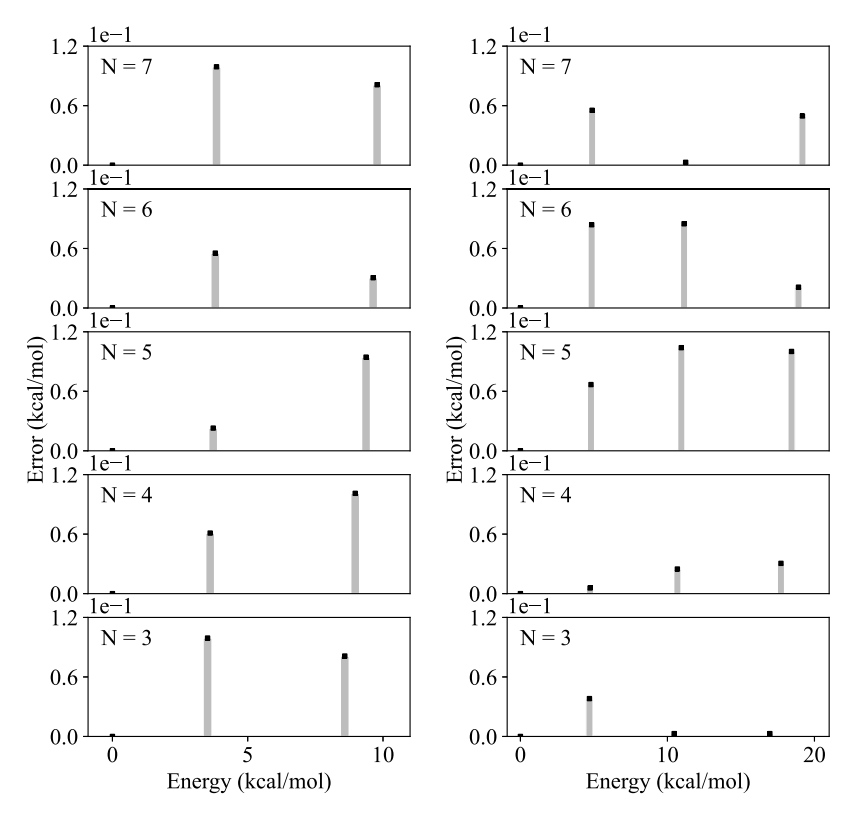


Figure 8. Eigenenergy differences between the classically computed (exact diagonalization) and QASM computed eigenenergies for the first three and four eigenvalues for  $H_5O_2^+$  (left) and  $H_3O_2^-$  (right).

treatment of electron correlation effects in conjunction with a rigorous treatment of quantum nuclear effects. 62,67,68,191–194

In this paper, we discuss (a) the Hamiltonian mapping protocol detailed in ref 138 and (b) a quantum circuit method based on the Quantum Shannon decomposition for simulating quantum nuclear dynamics. Using the two methods discussed here, we simulate the time evolution of the quantum nuclear wavepacket corresponding to the shared-proton degree of freedom in a short, strong hydrogen bond in small water clusters. The Hamiltonian mapping is a general but approximate mapping procedure between a quantum chemical dynamics problem, constructed on a single Born-Oppenheimer surface, and an ion-trap quantum simulator where the dynamics are dictated by a generalized form of a spin-lattice or Ising model Hamiltonian. This is exact for a small number of qubits, while it becomes approximate for a larger number of qubits with quantitative error measures. The quantum circuit decomposition technique, on the other hand, is in principle exact for a higher number of qubits, but practical implementation of the circuits remains a challenge for nearterm quantum architectures due to the exponential increase in the number of entangling gates in the circuit decomposition.

The key step involved in facilitating our Hamiltonian map is the partitioning of the coupled qubit space into two zones that we illustrate by using the q-sphere representation of the computational basis. Once the coupled qubit computational basis set is partitioned in such a way, the Ising model Hamiltonian reduces into a block form, thus allowing the possibility to map all problems that may be written in a similar block form. The Quantum Shannon decomposition method, on the other hand, reduces any arbitrary unitary state into a compact sequence of quantum gates from a universal gate set. The decomposition is also formally exact for an arbitrary

dimensional unitary. This can also treat chemical problems with arbitrary potential energy surfaces and yields a number of entangling gates close to the expected theoretical lower bound. Additionally, the QSD formalism has been shown to provide CNOT gate count close to the theoretical lower bound. 143

We consider intramolecular proton transfers in hydroxide and protonated water clusters and show how such problems can be mapped to an ion-trap system, and also show that the dynamics can be simulated using a quantum circuit decomposition method on a quantum simulator. General quantum nuclear dynamics problems, however, have unsymmetric potential energy surfaces and are generally performed in higher dimensions. Critical extensions to higher quantum nuclear dimensions have been implemented using tensor networks in refs 142 and 140. The methods discussed here will become critical in extending our mapping protocol to general potentials in higher dimensions, as will be considered in future publications.

### ASSOCIATED CONTENT

#### Supporting Information

The Supporting Information is available free of charge at https://pubs.acs.org/doi/10.1021/acs.jctc.4c01343.

Details regarding the unitary transforms that yield a block structure for the nuclear Hamiltonian and thus make the map between the ion-trap Hamiltonian and quantum nuclear Hamiltonian possible; electronic structure-based potential surfaces for  $H_3O_2^-$  and  $H_5O_2^+$ ; initial wavepacket details; a new correlation function idea to compute vibrational eigenenergies (that was introduced originally in ref 139); and more details on

the vibrational spectra obtained from quantum simulations (PDF)

#### AUTHOR INFORMATION

#### **Corresponding Author**

Srinivasan S. Iyengar — Department of Chemistry,
Department of Physics, and the Indiana University Quantum
Science and Engineering Center (IU-QSEC), Indiana
University, Bloomington, Indiana 47405, United States;
orcid.org/0000-0001-6526-2907; Email: iyengar@iu.edu

#### Authors

Debadrita Saha – Department of Chemistry, and the Indiana University Quantum Science and Engineering Center (IU-QSEC), Indiana University, Bloomington, Indiana 47405, United States

Philip Richerme – Department of Physics, and the Indiana University Quantum Science and Engineering Center (IU-QSEC), Indiana University, Bloomington, Indiana 47405, United States

Complete contact information is available at: https://pubs.acs.org/10.1021/acs.jctc.4c01343

#### **Notes**

The authors declare no competing financial interest.

#### ACKNOWLEDGMENTS

This research was supported by the National Science Foundation grants CHE-2102610 (S.S.I.), OMA-1936353 (S.S.I. and P.R.), and CHE-2311165 (S.S.I. and P.R.).

#### REFERENCES

- (1) Shin, J.-W.; Hammer, N. I.; Diken, E. G.; Johnson, M. A.; Walters, R. S.; Jaeger, T. D.; Duncan, M. A.; Christie, R. A.; Jordan, K. D. Infrared Signature of Structures Associated with the  $H^+(H_2O)_n$  (N = 6 to 27) Clusters. *Science* **2004**, 304, 1137.
- (2) Iyengar, S. S.; Petersen, M. K.; Day, T. J. F.; Burnham, C. J.; Teige, V. E.; Voth, G. A. The Properties of Ion-Water Clusters. I. the Protonated 21-Water Cluster. *J. Chem. Phys.* **2005**, *123*, 084309.
- (3) Iyengar, S. S. Further Analysis of the Dynamically Averaged Vibrational Spectrum for the "magic" Protonated 21-Water Cluster. *J. Chem. Phys.* **2007**, *126*, No. 216101.
- (4) Wu, C.-C.; Lin, C.-K.; Chang, H.-C.; Jiang, J.-C.; Kuo, J.-L.; Klein, M. L. Protonated Clathrate Cages Enclosing Neutral Water Molecules:  $H^+(H_2O)_{21}$  and  $H^+(H_2O)_{28}$ . J. Chem. Phys. **2005**, 122, No. 074315.
- (5) Asthagiri, D.; Pratt, L. R.; Kress, J. D.; Gomez, M. A. Hydration and Mobility of HO<sup>-</sup>(Aq). *Proc. Natl. Acad. Sci. U.S.A.* **2004**, *101*, 7229.
- (6) Tuckerman, M. E.; Marx, D.; Parrinello, M. The Nature and Transport Mechanism of Hydrated Hydroxide Ions in Aqueous Solution. *Nature* **2002**, *417*, 925.
- (7) Agmon, N. Mechanism of Hydroxide Mobility. Chem. Phys. Lett. 2000, 319, 247.
- (8) Diken, E. G.; Headrick, J. M.; Roscioli, J. R.; Bopp, J. C.; Johnson, M. A.; McCoy, A. B. Fundamental Excitations of the Shared Proton in the  $\rm H_3O_2^-$  and  $\rm H_5O_2^+$  Complexes. *J. Phys. Chem. A* **2005**, 109, 1487.
- (9) Robertson, W. H.; Diken, E. G.; Price, E. A.; Shin, J.-W.; Johnson, M. A. Spectroscopic Determination of the OH- Solvation Shell in the  $\mathrm{OH^-(H_2O)_n}$  Clusters. *Science* **2003**, 299, 1367.
- (10) Mundy, C. J.; Kuo, I.-F. W.; Tuckerman, M. E.; Lee, H.-S.; Tobias, D. J. Hydroxide anion at the air—water interface. *Chem. Phys. Lett.* **2009**, 481, 2.

- (11) Miyazaki, M.; Fujii, A.; Ebata, T.; Mikami, N. Infrared Spectroscopic Evidence for Protonated Water Clusters Forming Nanoscale Cages. *Science* **2004**, *304*, 1134.
- (12) Xiao, X.-D.; Vogel, V.; Shen, Y. R. Probing the Proton Excess at Interfaces by Second Harmonic Generation. *Chem. Phys. Lett.* **1989**, *163*, 555.
- (13) Radüge, C.; Pflumio, V.; Shen, Y. R. Surface Vibrational Spectroscopy of Sulfuric Acid-Water Mixtures at the Liquid-Vapor Interface. *Chem. Phys. Lett.* **1997**, 274, 140.
- (14) Achatz, U.; Fox, B. S.; Beyer, M. K.; Bondybey, V. E. Hypoiodous Acid As Guest Molecule in Protonated Water Clusters: A Combined FT-ICR/DFT Study of  $I(H_2O)^+_n$ . J. Am. Chem. Soc. **2001**, 123, 6151.
- (15) Lee, S.-W.; Cox, H.; Goddard, I. W. A.; Beauchamp, J. L. Chemistry in Nanodroplets: Studies of Protonation Sites of Substituted Anilines in Water Clusters Using FT-ICR. *J. Am. Chem. Soc.* **2000**, *122*, 9201.
- (16) Tuckerman, M. E.; Marx, D.; Klein, M. L.; Parrinello, M. On the Quantum Nature of the Shared Proton in Hydrogen Bonds. *Science* **1997**, *275*, 817–820.
- (17) Tuckerman, M. E.; Laasonen, K.; Sprik, M.; Parrinello, M. Ab Initio Molecular Dynamics Simulation of the Solvation and Transport of H<sub>3</sub>O<sup>+</sup> and OH<sup>-</sup> Ions in Water. *J. Phys. Chem. A* **1995**, *99*, 5749.
- (18) Sadhukhan, S.; Munoz, D.; Adamo, C.; Scuseria, G. E. Predicting Proton Transfer Barriers with Density Functional Methods. *Chem. Phys. Lett.* **1999**, *306*, 83.
- (19) Lobaugh, J.; Voth, G. A. The Quantum Dynamics of an Excess Proton in Water. J. Chem. Phys. 1996, 104, 2056.
- (20) McEwan, M. J.; Phillips, L. F. Chemistry of the Atmosphere; Eward Arnold: London, 1975.
- (21) Wayne, R. P. Chemistry of the Atmosphere; Clarendon Press: Oxford, 1994.
- (22) McEwan, M. J.; Phillips, L. F. Chemistry in the Upper Atmosphere. Acc. Chem. Res. 1970, 3, 9.
- (23) Teeter, M. M. Water Structure of a Hydrophobic Protein at Atomic Resolution: Pentagon Rings of Water Molecules in Crystals of Crambin. *Proc. Natl. Acad. Sci. U.S.A.* **1984**, *81*, 6014.
- (24) Neidle, S.; Berman, H. M.; Shieh, H. S. Highly Structured Water Network in Crystals of a Deoxydinucleoside-Drug Complex. *Nature* **1980**, 288, 129.
- (25) Lipscomb, L. A.; Peek, M. E.; Zhou, F. X.; Bertrand, J. A.; VanDerveer, D.; Williams, L. D. Water Ring Structure at Dna Interfaces Hydration and Dynamics of Dna Anthracycline Complexes. *Biochemistry* **1994**, *33*, 3649.
- (26) Cleland, W. W.; Kreevoy, M. M. Low-Barrier Hydrogen Bonds and Enzymic Catalysis. *Science* **1994**, *264*, 1887.
- (27) Warshel, A.; Papazyan, A.; Kollman, P. A. On Low-Barrier Hydrogen Bonds and Enzyme Catalysis. *Science* **1995**, *269* (5220), 102–106.
- (28) Marx, D.; Tuckerman, M. E.; Parrinello, M. Solvated Excess Protons in Water: Quantum Effects on the Hydration Structure. *J. Phys.; Condens. Matter* **2000**, *12*, A153.
- (29) Ricard, T. C.; Zhu, X.; Iyengar, S. S. Capturing weak interactions in surface adsorbate systems at coupled cluster accuracy: a graph-theoretic molecular fragmentation approach improved through machine learning. *J. Chem. Theory Comput.* **2023**, *19*, 8541.
- (30) Narayan, S.; Muldoon, J.; Finn, M.; Fokin, V.; Kolb, H.; Sharpless, K. On Water":Unique reactivity of organic compounds in aqueous suspension. *Angew. Chem., Int. Ed.* **2005**, *44*, 3275–3279.
- (31) Gajewski, J. J. The Claisen rearrangement. Response to solvents and substituents: The case for both hydrophobic and hydrogen bond acceleration in water and for a variable transition state. *Acc. Chem. Res.* **1997**, *30*, 219–225.
- (32) Breslow, R.; Maitra, U.; Rideout, D. Selective Diels-Alder Reactions In Aqueous-Solutions And Suspensions. *Tetrahedron Lett.* **1983**, *24*, 1901–1904.
- (33) Breslow, R.; Maitra, U. On The Origin Of Product Selectivity In Aqueous Diels-Alder Reactions. *Tetrahedron Lett.* **1984**, 25, 1239—1240.

- (34) Breslow, R. Hydrophobic Effects On Simple Organic-Reactions In Water. *Acc. Chem. Res.* **1991**, *24*, 159–164.
- (35) DE JONG, B. P. H. K.; Wilson, J. E.; Neilson, G. W.; Buckingham, A. D. Hydrophobic Hydration Of Methane. *Mol. Phys.* **1997**, *91*, 99–103.
- (36) Chanda, A.; Fokin, V. V. Synthesis "On Water". Chem. Rev. 2009, 109, 725-748.
- (37) Shapiro, N.; Vigalok, A. Highly Efficient Organic Reactions "On Water", "In Water", and both. *Angew. Chem., Int. Ed.* **2008**, 47, 2849–2852.
- (38) Huang, J.; Zhang, X.; Armstrong, D. W. Highly Efficient Asymmetric Direct Stoichiometric Aldol Reactions On/In Water. *Angew. Chem., Int. Ed.* **2007**, *46*, 9073–9077.
- (39) Turner, G. L.; Morris, J. A.; Greaney, M. F. Direct Arylation Of Thiazoles On Water. *Angew. Chem., Int. Ed.* **2007**, *46*, 7996–8000.
- (40) Wu, X.; Li, X.; Zanotti-Gerosa, A.; Pettman, A.; Liu, J.; Mills, A. J.; Xiao, J. Rh(III)- And Ir(III)-Catalyzed Asymmetric Transfer Hydrogenation Of Ketones In Water. *Chem.—Eur. J.* **2008**, *14*, 2209–2222.
- (41) Butler, R. N.; Coyne, A. G.; Cunningham, W. J.; Moloney, E. M. Water And Organic Synthesis: A Focus On The In-Water And On-Water Border. Reversal Of The In-Water Breslow Hydrophobic Enhancement Of The Normal Endo-Effect On Crossing To On-Water Conditions For Huisgen Cycloadditions With Increasingly Insoluble Organic Liquid And Solid  $2\pi$ -Dipolarophiles. *J. Org. Chem.* **2013**, 78, 3276–3291.
- (42) Davis, J. G.; Rankin, B. M.; Gierszal, K. P.; Ben-Amotz, D. On The Cooperative Formation Of Non-Hydrogen-Bonded Water At Molecular Hydrophobic Interfaces. *Nat. Chem.* **2013**, *5*, 796–802.
- (43) Jung, Y.; Marcus, R. A. On The Theory Of Organic Catalysis On Water. J. Am. Chem. Soc. 2007, 129, 5492-5502.
- (44) Jung, Y.; Marcus, R. A. Protruding Interfacial OH Groups And "On-Water" Heterogeneous Catalysis. *J. Phys.: Condens. Matter* **2010**, 22, No. 284117.
- (45) Wang, Y.; Hodas, N. O.; Jung, Y.; Marcus, R. A. Microscopic Structure And Dynamics Of Air/Water Interface By Computer Simulations-Comparison With Sum-Frequency Generation Experiments. *Phys. Chem. Chem. Phys.* **2011**, *13*, 5388–5393.
- (46) Kühne, T. D.; Pascal, T. A.; Kaxiras, E.; Jung, Y. New Insights Into The Structure Of The Vapor/Water Interface From Large-Scale First-Principles Simulations. *J. Phys. Chem. Lett.* **2011**, *2*, 105–113.
- (47) Karhan, K.; Khaliullin, R. Z.; Kuehne, T. D. On The Role Of Interfacial Hydrogen Bonds In "On-Water" Catalysis. *J. Chem. Phys.* **2014**, *141*, No. 22D528.
- (48) Kessler, J.; Elgabarty, H.; Spura, T.; Karhan, K.; Partovi-Azar, P.; Hassanali, A. A.; Kuehne, T. D. Structure And Dynamics Of The Instantaneous Water/Vapor Interface Revisited By Path-Integral And Ab Initio Molecular Dynamics Simulations. *J. Phys. Chem. B* **2015**, *119*, 10079–10086.
- (49) Schuster, M. F.; Meyer, W. H. Anhydrous Proton-Conducting Polymers. *Annu. Rev. Mater. Res.* **2003**, 33, 233.
- (50) Tse, Y.-L. S.; Herring, A. M.; Kim, K.; Voth, G. A. Molecular Dynamics Simulations of Proton Transport in 3M and Nafion Perfluorosulfonic Acid Membranes. *J. Phys. Chem. C* **2013**, *117*, 8079.
- (51) Roscioli, J. R.; McCunn, L. R.; Johnson, M. A. Quantum Structure of the Intermolecular Proton Bond. *Science* **2007**, *316*, 249.
- (52) Moore, D. T.; Oomens, J.; van der Meer, L.; von Helden, G.; Meijer, G.; Valle, J.; Marshall, A. G.; Eyler, J. R. Probing the Vibrations of Shared, OH<sup>+</sup>O-Bound Protons in the Gas Phase. *ChemPhysChem* **2004**, *5*, 740.
- (53) Headrick, J. M.; Diken, E. G.; Walters, R. S.; Hammer, N. I.; Christie, R. A.; Cui, J.; Myshakin, E. M.; Duncan, M. A.; Johnson, M. A.; Jordan, K. Spectral Signatures of Hydrated Proton Vibrations in Water Clusters. *Science* 2005, 308, 1765.
- (54) Valle, J. J.; Eyler, J. R.; Oomens, J.; Moore, D. T.; van der Meer, A. F. G.; von Helden, G.; Meijer, G.; Hendrickson, C. L.; Marshall, A. G.; Blakney, G. T. Free Electron Laser-Fourier Transform Ion Cyclotron Resonance Mass Spectrometry Facility for Obtaining

- Infrared Multiphoton Dissociation Spectra of Gaseous Ions. Rev. Sci. Instrum. 2005, 76, No. 023103, DOI: 10.1063/1.1841953.
- (55) Asmis, K. R.; Pivonka, N. L.; Santambrogio, G.; Brümmer, M.; Kaposta, C.; Neumark, D. M.; Wöste, L. Gas-Phase Infrared Spectrum of the Protonated Water Dimer. *Science* **2003**, 299, 1375.
- (56) Bush, M. F.; Forbes, M. W.; Jockusch, R. A.; Oomens, J.; Polfer, N. C.; Saykally, R.; Williams, E. Infrared Spectroscopy of Cationized Lysine and  $\varepsilon$ -N-Methyllysine in the Gas Phase: Effects of Alkali-Metal Ion Size and Proton Affinity on Zwitterion Stability. *J. Phys. Chem. A* **2007**, *111* (32), 7753–7760, DOI: 10.1021/jp071902q.
- (57) Pivonka, N. L.; Kaposta, C.; Brummer, M.; von Helden, G.; Meijer, G.; Woste, L.; Neumark, D. M.; Asmis, K. R. Probing a Strong Hydrogen Bond with Infrared Spectroscopy: Vibrational Predissociation of BrHBr-Ar. J. Chem. Phys. 2003, 118, 5275.
- (58) Vendrell, O.; Gatt18i, F.; Meyer, H.-D. Dynamics and Infrared Spectroscopy of the Protonated Water Dimer. *Angew. Chem. Int. Ed.* **2007**, *46*, 6918.
- (59) Vendrell, O.; Gatti, F.; Meyer, H.-D. Full Dimensional (15D) Quantum-Dynamical Simulation of the Protonated Water-Dimer. II. Infrared Spectrum and Vibrational Dynamics. *J. Chem. Phys.* **2007**, 127, No. 184303.
- (60) Vendrell, O.; Gatti, F.; Meyer, H.-D. Strong Isotope Effects in the Infrared Spectrum of the Zundel Cation. *Angew. Chem., Int. Ed.* **2009**, *48*, 352.
- (61) Hammer, N. I.; Diken, E. G.; Roscioli, J. R.; Johnson, M. A.; Myshakin, E. M.; Jordan, K. D.; McCoy, A. B.; Huang, X.; Bowman, J. M.; Carter, S. The Vibrational Predissociation Spectra of the  $H_5O_2^+$ ·RG<sub>n</sub>(RG = Ar,Ne) clusters: Correlation of the solvent perturbations in the free OH and shared proton transitions of the Zundel ion. *J. Chem. Phys.* **2005**, *122*, No. 244301.
- (62) Nagel, Z. D.; Klinman, J. Tunneling and Dynamics in Enzymatic Hydride Transfer. *Chem. Rev.* **2006**, *106*, 3095.
- (63) Soudackov, A. V.; Hammes-Schiffer, S. Probing Non-adiabaticity in the Proton-Coupled Electron Transfer Reaction Catalyzed by Soybean Lipoxygenase. *J. Phys. Chem. Lett.* **2014**, *5*, 3274.
- (64) Hynes, J. T.; Klinman, J. P.; Limbach, H.-H.; Schowen, R. L. *Hydrogen-Transfer Reactions*; Eds.; Wiley-VCH: Weinheim, Germany, 2007.
- (65) Cukier, R. I.; Nocera, D. G. Proton-coupled electron transfer. *Annu. Rev. Phys. Chem.* **1998**, *49*, 337–369.
- (66) Mayer, J. M. Proton-coupled electron transfer: A Reaction Chemist's View. *Annu. Rev. Phys. Chem.* **2004**, *55*, 363–390.
- (67) Iyengar, S. S.; Sumner, I.; Jakowski, J. Hydrogen Tunneling in an Enzyme Active Site: A Quantum Wavepacket Dynamical Perspective. *J. Phys. Chem. B* **2008**, *112*, 7601.
- (68) Sumner, I.; Iyengar, S. S. Analysis of Hydrogen Tunneling in an Enzyme Active Site Using Von Neumann Measurements. *J. Chem. Theory Comput.* **2010**, *6*, 1698.
- (69) Hammerich, A. D.; Manthe, U.; Kosloff, R.; Meyer, H.; Cederbaum, L. S. Time-dependent photodissociation of methyl iodide with five active modes. *J. Chem. Phys.* **1994**, *101*, 5623–5646.
- (70) Manthe, U.; Meyer, H. D.; Cederbaum, L. S. Wave-packet dynamics within the multiconfiguration Hartree framework: General aspects and application to NOCl. *J. Chem. Phys.* **1992** *97*, 3199–3213.
- (71) Beck, M. H.; Jäckle, A.; Worth, G. A.; Meyer, H.-D. The multiconfiguration time-dependent Hartree (MCTDH) method: a highly efficient algorithm for propagating wavepackets. *Phys. Rep.* **2000**, 324, 1–105.
- (72) Pasin, G.; Iung, C.; Gatti, F.; Meyer, H. D. Theoretical Investigation of Highly Excited Vibrational States in DFCO: Calculation of the Out-Of-Plane Bending States and Simulation of the Intramolecular Vibrational Energy Redistribution. *J. Chem. Phys.* **2007**, *126*, No. 024302, DOI: 10.1063/1.2402920.
- (73) Bowman, J. M. The Self-Consistent-Field Approach to Polyatomic Vibrations. Acc. Chem. Res. 1986, 19, 202.
- (74) McCoy, A. B.; Gerber, R. B.; Ratner, M. A. A Quantitative Approximation for the Quantum Dynamics of Hydrogen Transfer:

- Transition State Dynamics and Decay in ClHCl<sup>-</sup>. *J. Chem. Phys.* **1994**, *101*, 1975.
- (75) Vendrell, O.; Gatti, F.; Meyer, H.-D. Dynamics and Infrared Spectroscopy of the Protonated Water Dimer. *Angew. Chem., Int. Ed.* **2007**, *46*, 6918.
- (76) Kaledin, M.; Kaledin, A. L.; Bowman, J. M. Vibrational Analysis of the  $H_5O_2^+$  Infrared Spectrum Using Molecular and Driven Molecular Dynamics. *J. Phys. Chem. A* **2006**, *110*, 2933.
- (77) McCoy, A. B.; Huang, X.; Carter, S.; Bowman, J. M. Quantum Studies of the Vibrations in  $H_3O_2^-$  and  $D_3O_2^-$ . *J. Chem. Phys.* **2005**, 123, No. 064317.
- (78) Pople, J. A.; Raghavachari, K.; Schlegel, H. B.; Binkley, J. S. Derivative Studies in Hartree-Fock and Møller-Plesset Theories. *Int. J. Quantum Chem.* **1979**, *16* (S13), 225–241.
- (79) Pople, J. A.; Schlegel, H. B.; Raghavachari, K.; DeFrees, D. J.; Binkley, J. S.; Frisch, M. J.; Whiteside, R. A.; Hout, R. F.; Hehre, W. J. Molecular orbital studies of vibrational frequencies. *Int. J. Quantum Chem.* **2009**, 20, 269–278.
- (80) Sumner, I.; Iyengar, S. S. Quantum Wavepacket Ab Initio Molecular Dynamics: An Approach for Computing Dynamically Averaged Vibrational Spectra Including Critical Nuclear Quantum Effects. J. Phys. Chem. A 2007, 111, 10313.
- (81) Li, X.; Oomens, J.; Eyler, J. R.; Moore, D. T.; Iyengar, S. S. Isotope Dependent, Temperature Regulated, Energy Repartitioning in a Low-Barrier, Short-Strong Hydrogen Bonded Cluster. *J. Chem. Phys.* **2010**, *1*32, No. 244301.
- (82) Iyengar, S. S.; Parker, G. A.; Kouri, D. J.; Hoffman, D. K. Symmetry-Adapted Distributed Approximating Functionals: Theory and Application to the Ro-Vibrational States of H<sub>3</sub>. *J. Chem. Phys.* **1999**, *110*, No. 10283.
- (83) Schlegel, H. B.; Frisch, M. J. Computational bottlenecks in molecular orbital calculations. In *Theoretical and Computational Models for Organic Chemistry*; Springer, 1991; pp 5–33.
- (84) Wyatt, R. E.; Zhang, J. Z. H. Dynamics of Molecules and Chemical Reactions; Eds.; Marcel Dekker Inc.: New York, NY, 1996.
- (85) Feynman, R. P.; Hibbs, A. R. Quantum Mechanics and Path Integrals; McGraw-Hill Book Company: New York, 1965.
- (86) Meyer, H.-D.; Manthe, U.; Cederbaum, L. S. The multiconfigurational time-dependent Hartree approach. *Chem. Phys. Lett.* **1990**, *165*, 73–78.
- (87) Nielsen, M. A.; Chuang, I. L. Quantum computation and quantum information; Cambridge University Press: Cambridge, 2000.
- (88) Feynman, R. P.; Hey, J.; Allen, R. W. Feynman Lectures on Computation; Addison-Wesley Longman Publishing Co., Inc., 1998.
- (89) Berman, L. The complexity of logical theories. *Theor. Comput. Sci.* **1980**, *11*, 71–77.
- (90) Deumens, E.; Diz, A.; Longo, R.; Öhrn, Y. Time-Dependent Theoretical Treatments of the Dynamics of Electrons and Nuclei in Molecular-Systems. *Rev. Mod. Phys.* **1994**, *66*, 917.
- (91) Kuppermann, A. The Geometric Phase in Reaction Dynamics. In *Dynamics of Molecules and Chemical Reactions*; Wyatt, R. E.; Zhang, J. Z. H., Eds.; Marcel Dekker Inc.: New York, NY, 1996; p 411.
- (92) Tal-Ezer, H.; Kosloff, R. An accurate and efficient scheme for propagating the time dependent Schrödinger equation. *J. Chem. Phys.* **1984**, *81*, 3967.
- (93) Kouri, D. J.; Zhu, W.; Ma, X.; Pettitt, B. M.; Hoffman, D. K. Monte Carlo evaluation of real-time Feynman path integrals for quantal many-body dynamics: distributed approximating functions and Gaussian sampling. *J. Phys. Chem. A* **1992**, *96* (24), 9622–9630, DOI: 10.1021/j100203a013.
- (94) Habershon, S.; Manolopoulos, D. E.; Markland, T. E.; Miller, T. F. Ring polymer molecular dynamics: Quantum effects in chemical dynamics from classical trajectories in an extended phase space. *Annu. Rev. Phys. Chem.* **2013**, *64*, 387.
- (95) DeGregorio, N.; Iyengar, S. S. Adaptive Dimensional Decoupling for Compression of Quantum Nuclear Wave Functions and Efficient Potential Energy Surface Representations through Tensor Network Decomposition. *J. Chem. Theory Comput.* **2019**, 15, 2780–2796.

- (96) DeGregorio, N.; Iyengar, S. S. Efficient and Adaptive Methods for Computing Accurate Potential Surfaces for Quantum Nuclear Effects: Applications to Hydrogen- Transfer Reactions. *J. Chem. Theory Comput.* **2018**, *14*, 30–47.
- (97) Ayala, P.; Scuseria, G. Linear scaling second-order Moller-Plesset theory in the atomic orbital basis for large molecular systems. *J. Chem. Phys.* **1999**, *110*, 3660.
- (98) Schütz, M.; Werner, H. Low-order scaling local electron correlation methods. IV. Linear scaling local coupled-cluster (LCCSD). J. Chem. Phys. 2001, 114, 661.
- (99) Distasio, R. A., Jr; Steele, R. P.; Rhee, Y. M.; Shao, Y.; Head-Gordon, M. An improved algorithm for analytical gradient evaluation in resolution-of-the-identity second-order M?ller-Plesset perturbation theory: Application to alanine tetrapeptide conformational analysis. *J. Comput. Chem.* **2007**, *28*, 839.
- (100) Pavošević, F.; Pinski, P.; Riplinger, C.; Neese, F.; Valeev, E. F. SparseMaps—A systematic infrastructure for reduced-scaling electronic structure methods. IV. Linear-scaling second-order explicitly correlated energy with pair natural orbitals. *J. Chem. Phys.* **2016**, *144*, No. 144109.
- (101) Haycraft, C.; Li, J.; Iyengar, S. S. Efficient, "On-the-fly" Born—Oppenheimer and Car—Parrinello—type Dynamics with coupled cluster accuracy through Fragment Based Electronic Structure. *J. Chem. Theory Comput.* **2017**, *13*, No. 21887.
- (102) Iyengar, S. S.; Kouri, D. J.; Hoffman, D. K. Particular and Homogeneous Solutions of Time-Independent Wavepacket Schrodinger Equations: Calculations Using a Subset of Eigenstates of Undamped or Damped Hamiltonians. *Theor. Chem. Acc.* 2000, 104, 471.
- (103) Skone, J. H.; Pak, M. V.; Hammes-Schiffer, S. Nuclear-Electronic Orbital Nonorthogonal Configuration Interaction Approach. *J. Chem. Phys.* **2005**, 123, No. 134108.
- (104) Iyengar, S. S.; Jakowski, J. Quantum Wavepacket Ab Initio Molecular Dynamics: An Approach to Study Quantum Dynamics in Large Systems. *J. Chem. Phys.* **2005**, *122*, No. 114105.
- (105) Binder, R.; Burghardt, I. First-principles description of intrachain exciton migration in an oligo(para-phenylene vinylene) chain. II ML-MCTDH simulations of exciton dynamics at a torsional defect. *J. Chem. Phys.* **2020**, *152*, No. 204120.
- (106) Kumar, A.; Iyengar, S. S. Fragment-based electronic structure for potential energy surfaces using a superposition of fragmentation topologies. *J. Chem. Theory Comput.* **2019**, *15*, 5769.
- (107) Abrams, D. S.; Lloyd, S. Simulation of many-body Fermi systems on a universal quantum computer. *Phys. Rev. Lett.* **1997**, 79, 2586
- (108) Aspuru-Guzik, A.; Dutoi, A. D.; Love, P. J.; Head-Gordon, M. Simulated quantum computation of molecular energies. *Science* **2005**, 309, 1704.
- (109) Wang, H.; Kais, S.; Aspuru-Guzik, A.; Hoffmann, M. R. Quantum algorithm for obtaining the energy spectrum of molecular systems. *Phys. Chem. Chem. Phys.* **2008**, *10*, 5388–5393.
- (110) Wecker, D.; Hastings, M. B.; Troyer, M. Progress towards practical quantum variational algorithms. *Phys. Rev. A* **2015**, *92*, No. 042303.
- (111) McClean, J. R.; Romero, J.; Babbush, R.; Aspuru-Guzik, A. The theory of variational hybrid quantum-classical algorithms. *New J. Phys.* **2016**, *18*, No. 023023.
- (112) O'Malley, P. J. J.; Babbush, R.; Kivlichan, I. D.; Romero, J.; McClean, J. R.; Barends, R.; Kelly, J.; Roushan, P.; Tranter, A.; Ding, N.; Campbell, B.; Chen, Y.; Chen, Z.; Chiaro, B.; Dunsworth, A.; Fowler, A. G.; Jeffrey, E.; Lucero, E.; Megrant, A.; Mutus, J. Y.; Neeley, M.; Neill, C.; Quintana, C.; Sank, D.; Vainsencher, A.; Wenner, J.; White, T. C.; Coveney, P. V.; Love, P. J.; Neven, H.; Aspuru-Guzik, A.; Martinis, J. M. Scalable Quantum Simulation of Molecular Energies. *Phys. Rev. X* **2016**, *6*, No. 031007.
- (113) Parrish, R. M.; Hohenstein, E. G.; McMahon, P. L.; Martinez, T. J. Quantum Computation of Electronic Transitions Using a Variational Quantum Eigensolver. *Phys. Rev. Lett.* **2019**, *122*, No. 230401.

- (114) Zhang, J. H.; Iyengar, S. S. Graph- $|Q\rangle\langle C|$ : A Graph-based Quantum-classical algorithm for efficient electronic structure on hybrid quantum/classical hardware systems: Improved quantum circuit depth performance. *J. Chem. Theory Comput.* **2022**, *18*, 2885. (115) Smart, S. E.; Mazziotti, D. A. Quantum solver of contracted eigenvalue equations for scalable molecular simulations on quantum computing devices. *Phys. Rev. Lett.* **2021**, *126*, No. 070504.
- (116) Iyengar, S. S.; Saha, D.; Dwivedi, A.; Lopez-Ruiz, M. A.; Kumar, A.; Zhang, J. H.; Ricard, T. C.; Richerme, P.; Sabry, A. Quantum Algorithms for the Study of Electronic Structure and Molecular Dynamics: Novel Computational Protocols. In *Comprehensive Computational Chemistry*; Elsevier, 2023.
- (117) Iyengar, S. S.; Zhang, J. H.; Saha, D.; Ricard, T. C. Graph-l Q\\Cl: A Quantum Algorithm with Reduced Quantum Circuit Depth for Electronic Structure. *J. Phys. Chem. A* **2023**, *127*, 9334.
- (118) Lanyon, B. P.; Whitfield, J. D.; Gillett, G. G.; Goggin, M. E.; Almeida, M. P.; Kassal, I.; Biamonte, J. D.; Mohseni, M.; Powell, B. J.; Barbieri, M.; Aspuru-Guzik, A.; White, A. G. Towards quantum chemistry on a quantum computer. *Nature Chem.* **2010**, *2*, 106–111. (119) Lu, D.; Xu, N.; Xu, R.; Chen, H.; Gong, J.; Peng, X.; Du, J. Simulation of chemical isomerization reaction dynamics on a NMR quantum simulator. *Phys. Rev. Lett.* **2011**, *107*, No. 020501.
- (120) Peruzzo, A.; McClean, J.; Shadbolt, P.; Yung, M.-H.; Zhou, X.-Q.; Love, P. J.; Aspuru-Guzik, A.; O'brien, J. L. A variational eigenvalue solver on a photonic quantum processor. *Nat. Commun.* 2014, 5, No. 4213.
- (121) Kandala, A.; Mezzacapo, A.; Temme, K.; Takita, M.; Brink, M.; Chow, J. M.; Gambetta, J. M. Hardware-efficient variational quantum eigensolver for small molecules and quantum magnets. *Nature* **2017**, *549*, 242.
- (122) Hempel, C.; Maier, C.; Romero, J.; McClean, J.; Monz, T.; Shen, H.; Jurcevic, P.; Lanyon, B. P.; Love, P.; Babbush, R.; Aspuru-Guzik, A.; Blatt, R.; Roos, C. F. Quantum Chemistry Calculations on a Trapped-Ion Quantum Simulator. *Phys. Rev. X* 2018, 8, No. 031022. (123) Nam, Y.; Chen, J.-S.; Pisenti, N. C.; Wright, K.; Delaney, C.; Maslov, D.; Brown, K. R.; Allen, S.; Amini, J. M.; Apisdorf, J.; Beck, K. M.; Blinov, A.; Chaplin, V.; Chmielewski, M.; Collins, C.; Debnath, S.; Hudek, K. M.; Ducore, A. M.; Keesan, M.; Kreikemeier, S. M.; Mizrahi, J.; Solomon, P.; Williams, M.; Wong-Campos, J. D.; Moehring, D.; Monroe, C.; Kim, J. Ground-state energy estimation of the water molecule on a trapped-ion quantum computer. *npj Quantum Inf.* 2020, 6, No. 33.
- (124) Arute, F.; Arya, K.; Babbush, R.; Bacon, D.; Bardin, J. C.; Barends, R.; Boixo, S.; Broughton, M.; Buckley, B. B.; Buell, D. A.; Burkett, B.; Bushnell, N.; Chen, Y.; Chen, Z.; Chiaro, B.; Collins, R.; Courtney, W.; Demura, S.; Dunsworth, A.; Farhi, E.; Fowler, A.; Foxen, B.; Gidney, C.; Giustina, M.; Graff, R.; Habegger, S.; Harrigan, M. P.; Ho, A.; Hong, S.; Huang, T.; Huggins, W. J.; Ioffe, L.; Isakov, S. V.; Jeffrey, E.; Jiang, Z.; Jones, C.; Kafri, D.; Kechedzhi, K.; Kelly, J.; Kim, S.; Klimov, P. V.; Korotkov, A.; Kostritsa, F.; Landhuis, D.; Laptev, P.; Lindmark, M.; Lucero, E.; Martin, O.; Martinis, J. M.; McClean, J. R.; McEwen, M.; Megrant, A.; Mi, X.; Mohseni, M.; Mruczkiewicz, W.; Mutus, J.; Naaman, O.; Neeley, M.; Neill, C.; Neven, H.; Niu, M. Y.; O'Brien, T. E.; Ostby, E.; Petukhov, A.; Putterman, H.; Quintana, C.; Roushan, P.; Rubin, N. C.; Sank, D.; Satzinger, K. J.; Smelyanskiy, V.; Strain, D.; Sung, K. J.; Szalay, M.; Takeshita, T. Y.; Vainsencher, A.; White, T.; Wiebe, N.; Yao, Z. J.; Yeh, P.; Zalcman, A. Hartree-Fock on a superconducting qubit quantum computer. Science 2020, 369, 1084-1089.
- (125) Sparrow, C.; Martín-López, E.; Maraviglia, N.; Neville, A.; Harrold, C.; Carolan, J.; Joglekar, Y. N.; Hashimoto, T.; Matsuda, N.; O'Brien, J. L.; Tew, D. P.; Laing, A. Simulating the vibrational quantum dynamics of molecules using photonics. *Nature* **2018**, 557, 660–667.
- (126) Wang, C. S.; Curtis, J. C.; Lester, B. J.; Zhang, Y.; Gao, Y. Y.; Freeze, J.; Batista, V. S.; Vaccaro, P. H.; Chuang, I. L.; Frunzio, L.; Jiang, L.; Girvin, S. M.; Schoelkopf, R. J. Efficient Multiphoton Sampling of Molecular Vibronic Spectra on a Superconducting Bosonic Processor. *Phys. Rev. X* **2020**, *10*, No. 021060.

- (127) Huh, J.; Guerreschi, G. G.; Peropadre, B.; McClean, J. R.; Aspuru-Guzik, A. Boson sampling for molecular vibronic spectra. *Nat. Photonics* **2015**, *9*, 615–620.
- (128) Wang, Y.; Sager-Smith, L. M.; Mazziotti, D. A. Quantum Simulation of Bosons with the Contracted Quantum Eigensolver. *New J. Phys* **2023**, 25, No. 103005, DOI: 10.1088/1367-2630/acf9c3.
- (129) Wang, C. S.; Frattini, N. E.; Chapman, B. J.; Puri, S.; Girvin, S. M.; Devoret, M. H.; Schoelkopf, R. J. Observation of Wave-Packet Branching through an Engineered Conical Intersection. *Phys. Rev. X* **2023**, *13*, No. 011008.
- (130) Valahu, C. H.; Olaya-Agudelo, V. C.; MacDonell, R. J.; Navickas, T.; Rao, A. D.; Millican, M. J.; Pérez-Sánchez, J. B.; Yuen-Zhou, J.; Biercuk, M. J.; Hempel, C.; Tan, T. R.; Ivan, K. Direct observation of geometric-phase interference in dynamics around a conical intersection. *Nat. Chem.* **2023**, *15*, 1503–1508.
- (131) Whitlow, J.; Jia, Z.; Wang, Y.; Fang, C.; Kim, J.; Brown, K. R. Quantum simulation of conical intersections using trapped ions. *Nat. Chem.* **2023**, *15*, 1509–1514.
- (132) Gambetta, F. M.; Zhang, C.; Hennrich, M.; Lesanovsky, I.; Li, W. Exploring the many-body dynamics near a conical intersection with trapped Rydberg ions. *Phys. Rev. Lett.* **2021**, *126*, No. 233404.
- (133) Navickas, T.; MacDonell, R. J.; Valahu, C. H.; Olaya-Agudelo, V. C.; Scuccimarra, F.; Millican, M. J.; Matsos, V. G.; Nourse, H. L.; Rao, A. D.; Biercuk, M. J.; Hempel, C.; Kassal, I.; Tan, T. R. Experimental Quantum Simulation of Chemical Dynamics. 2024; https://arxiv.org/abs/2409.04044.
- (134) Wang, Y.; Mazziotti, D. A. Quantum simulation of conical intersections. *Phys. Chem. Chem. Phys.* **2024**, 26, 11491–11497.
- (135) Xing, X.; Gomez Cadavid, A.; Izmaylov, A. F.; Tscherbul, T. V. A hybrid quantum-classical algorithm for multichannel quantum scattering of atoms and molecules. *J. Phys. Chem. Lett.* **2023**, *14*, 6224–6233.
- (136) Kale, S. S.; Kais, S. Simulation of Chemical Reactions on a Quantum Computer. J. Phys. Chem. Lett. 2024, 15, 5633-5642.
- (137) Dietrick, S. M.; Iyengar, S. S. Constructing Periodic Phase Space Orbits from Ab Initio Molecular Dynamics Trajectories to Analyze Vibrational Spectra: Case Study of the Zundel  $(H_5O_2^+)$  Cation. *J. Chem. Theory Comput.* **2012**, *8*, 4876.
- (138) Saha, D.; Iyengar, S. S.; Richerme, P.; Smith, J. M.; Sabry, A. Mapping Quantum Chemical Dynamics Problems to Spin-Lattice Simulators. *J. Chem. Theory Comput.* **2021**, *17*, 6713–6732.
- (139) Richerme, P.; Revelle, M. C.; Yale, C. G.; Lobser, D.; Burch, A. D.; Clark, S. M.; Saha, D.; Lopez-Ruiz, M. A.; Dwivedi, A.; Smith, J. M.; et al. Quantum computation of hydrogen bond dynamics and vibrational spectra. *J. Phys. Chem. Lett.* **2023**, *14*, 7256–7263.
- (140) Dwivedi, A.; Rasmussen, A. J.; Richerme, P.; Iyengar, S. S. Quantum nuclear dynamics on a distributed set of ion-trap quantum computing systems. *J. Am. Chem. Soc.* **2024**, *146*, 29355–29363.
- (141) Saha, D. Development and Implementation of Quantum Computing Algorithms for the Study of Quantum Nuclear Dynamics and vibrational spectroscopy. Ph.D. thesis, Indiana University, 2024.
- (142) Dwivedi, A.; Lopez-Ruiz, M. A.; Iyengar, S. S. Resource Optimization for Quantum Dynamics with Tensor Networks: Quantum and Classical Algorithms. *J. Phys. Chem. A* **2024**, *128*, 6774–6797.
- (143) Shende, V.; Bullock, S.; Markov, I. Synthesis of quantum-logic circuits. *IEEE Trans. Computer-Aided Des. Integr. Circuits Syst.* **2006**, 25, 1000–1010.
- (144) Cleland, W. W.; Kreevoy, M. M. Low-Barrier Hydrogen Bonds and Enzymic Catalysis. *Science* **1994**, 264, 1887.
- (145) Chatfield, D. C.; Brooks, B. R. HIV-1 Protease Cleavage Mechanism Elucidated with Molecular Dynamics Simulation. *J. Am. Chem. Soc.* **1995**, *117*, 5561.
- (146) Warshel, A.; Papazyan, A.; Kollman, P. A. On Low-Barrier Hydrogen-Bonds and Enzyme Catalysis. *Science* **1995**, *269*, 102.
- (147) Perrin, C. L.; Nielson, J. B. 'Strong' Hydrogen Bonds in Chemistry and Biology. *Ann. Rev. Phys. Chem.* **1997**, *48*, 511.
- (148) Li, X.; Teige, V. E.; Iyengar, S. S. Can the Four-Coordinated, Penta-Valent Oxygen in Hydroxide Water Clusters Be Detected

- Through Experimental Vibrational Spectroscopy? J. Phys. Chem. A 2007, 111, 4815.
- (149) Iyengar, S. S.; Li, X.; Sumner, I. The Study of Dynamically Averaged Vibrational Spectroscopy of Atmospherically Relevant Clusters Using Ab Initio Molecular Dynamics in Conjunction with Quantum Wavepackets. *Adv. Quantum Chem.* **2008**, *55*, 333.
- (150) Hudson, B. S.; Verdal, N. Vibrational Dynamics in Short, Strong Symmetric Hydrogen Bonds: General Considerations and Two Examples. *Phys. B: Condens. Matter* **2006**, 385-386, 212.
- (151) Chisholm, C. R. I.; Haile, S. M. Entropy Evaluation of the Superprotonic Phase of CsHSO<sub>4</sub>: Pauling's Ice Rules Adjusted for Systems Containing Disordered Hydrogen-Bonded Tetrahedra. *Chem. Mater.* **2007**, *19*, 270.
- (152) Haile, S. M.; Chisholm, C. R. I.; Sasaki, K.; Boysen, D. A.; Uda, T. Solid Acid Proton Conductors: From Laboratory Curiosities to Fuel Cell Electrolytes. *Faraday Discuss.* **2007**, *134*, 17.
- (153) Suzuki, K.; Hayashi, S. H-1 NMR Study of Proton Dynamics in  $Cs_5H_3(SO_4)_4 \times H_2O$ . *Phys. Rev. B* **2006**, 74, No. 134303, DOI: 10.1103/PhysRevB.74.134303.
- (154) Xia, R.; Bian, T.; Kais, S. Electronic Structure Calculations and the Ising Hamiltonian. *J. Phys. Chem. B* **2018**, *122*, 3384–3395.
- (155) Jordan, P.; Wigner, E. Über das Paulische Äquivalenzverbot. Z. Phys. 1928, 47, 631–651.
- (156) Lill, J. V.; Parker, G. A.; Light, J. C. Discrete Variable Representations and Sudden Models in Quantum Scattering-Theory. *Chem. Phys. Lett.* **1982**, *89*, 483.
- (157) Huang, Y.; Kouri, D. J.; Arnold, M.; Thomas, L.; Marchioro, I.; Hoffman, D. K. Distributed Approximating Function Approach to Time-Dependent Wavepacket Propagation in 3-Dimensions: Atom-Surface Scattering. *Comput. Phys. Commun.* **1994**, *80*, 1–16.
- (158) Olmschenk, S.; Younge, K. C.; Moehring, D. L.; Matsukevich, D. N.; Maunz, P.; Monroe, C. Manipulation and detection of a trapped Yb+ hyperfine qubit. *Phys. Rev. A* **2007**, *76*, No. 052314.
- (159) Onsager, L. Crystal Statistics. I. A Two-Dimensional Model with an Order-Disorder Transition. *Phys. Rev.* **1944**, *65*, 117–149.
- (160) McCoy, B. M.; Wu, T. T. The Two-Dimensional Ising Model; Harvard University Press: Cambridge, MA and London, England, 1973.
- (161) Wilson, K. G. Renormalization Group and Critical Phenomena. I. Renormalization Group and the Kadanoff Scaling Picture. *Phys. Rev. B* **1971**, *4*, 3174–3183.
- (162) Anderson, F. B.; Callen, H. B. Statistical Mechanics and Field-Induced Phase Transitions of the Heisenberg Antiferromagnet. *Phys. Rev.* **1964**, *136*, A1068–A1087.
- (163) Cohen, E.; Tamir, B. D-Wave and predecessors: From simulated to quantum annealing. *Int. J. Quantum Inf.* **2014**, *12*, No. 1430002.
- (164) Johnson, M. W.; Amin, M. H. S.; Gildert, S.; Lanting, T.; Hamze, F.; Dickson, N.; Harris, R.; Berkley, A. J.; Johansson, J.; Bunyk, P.; Chapple, E. M.; Enderud, C.; Hilton, J. P.; Karimi, K.; Ladizinsky, E.; Ladizinsky, N.; Oh, T.; Perminov, I.; Rich, C.; Thom, M. C.; Tolkacheva, E.; Truncik, C. J. S.; Uchaikin, S.; Wang, J.; Wilson, B.; Rose, G. Quantum annealing with manufactured spins. *Nature* 2011, 473, 194–198.
- (165) Lechner, W.; Hauke, P.; Zoller, P. A quantum annealing architecture with all-to-all connectivity from local interactions. *Sci. Adv.* **2015**, *1*, No. e1500838.
- (166) Javadi-Abhari, A.; Treinish, M.; Krsulich, K.; Wood, C. J.; Lishman, J.; Gacon, J.; Martiel, S.; Nation, P. D.; Bishop, L. S.; Cross, A. W.; Johnson, B. R.; Gambetta, J. M. Quantum computing with Qiskit 2024 https://arxiv.org/abs/2405.08810.
- (167) Kouri, D. J.; Huang, Y.; Hoffman, D. K. Iterated Real-Time Path Integral Evaluation Using a Distributed Approximating Functional Propagator and Average-Case Complexity Integration. *Phys. Rev. Lett.* **1995**, *75*, 49.
- (168) Hoffman, D. K.; Nayar, N.; Sharafeddin, O. A.; Kouri, D. J. Analytic Banded Approximation for the Discretized Free Propagator. *J. Phys. Chem. A* **1991**, 95, 8299.

- (169) Golub, G. H.; Van Loan, C. F. Matrix Computations; JHU Press, 2013; Vol. 3.
- (170) Barenco, A.; Bennett, C. H.; Cleve, R.; DiVincenzo, D. P.; Margolus, N.; Shor, P.; Sleator, T.; Smolin, J. A.; Weinfurter, H. Elementary gates for quantum computation. *Phys. Rev. A* **1995**, *52*, 3457.
- (171) Möttönen, M.; Vartiainen, J. J. Decompositions of general quantum gates. In *Trends in quantum computing research* 2006; pp 149–170.
- (172) Golub, G. H.; Loan, C. F. V. *Matrix Computations*; The Johns Hopkins University Press: Baltimore, 1996.
- (173) Sutton, B. D. Computing the complete CS decomposition. *Numerical Algorithms* **2009**, *50*, 33–65.
- (174) Paige, C. C.; Wei, M. History and generality of the CS decomposition. *Linear Algebra Appl.* **1994**, 208-209, 303–326.
- (175) Möttönen, M.; Vartiainen, J. J.; Bergholm, V.; Salomaa, M. M. Quantum circuits for general multiqubit gates. *Phys. Rev. Lett.* **2004**, 93, No. 130502.
- (176) Chia, N.-H.; Chung, K.-M.; Lai, C.-Y. On the Need for Large Quantum Depth. In *Proceedings of the 52nd Annual ACM SIGACT Symposium on Theory of Computing. STOC* 2020; Association for Computing Machinery: New York, NY, USA, 2020; pp 902–915.
- (177) Preskill, J. Quantum Computing in the NISQ era and beyond. *Quantum* **2018**, 2, 79.
- (178) Baciou, L.; Michel, H. Interruption of the water chain in the reaction center from Rhodobacter sphaeroides reduces the rates of the proton uptake and of the second electron transfer to QB. *Biochemistry* **1995**, *34*, 7967–7972.
- (179) Guo, H.; Barnard, A. S. Proton transfer in the hydrogenbonded chains of lepidocrocite: a computational study. *Phys. Chem. Chem. Phys.* **2011**, *13*, No. 17864.
- (180) Domene, C.; Sansom, M. S. Potassium channel, ions, and water: simulation studies based on the high resolution X-ray structure of KcsA. *Biophys. J.* **2003**, *85*, 2787–2800.
- (181) Mann, D. J.; Halls, M. D. Water Alignment and Proton Conduction inside Carbon Nanotubes. *Phys. Rev. Lett.* **2003**, *90*, No. 195503.
- (182) Song, W.; Joshi, H.; Chowdhury, R.; Najem, J. S.; Shen, Y.-X.; Lang, C.; Henderson, C. B.; Tu, Y.-M.; Farell, M.; Pitz, M. E.; et al. Artificial water channels enable fast and selective water permeation through water-wire networks. *Nat. Nanotechnol.* **2020**, *15*, 73–79.
- (183) Hummer, G.; Rasaiah, J. C.; Noworyta, J. P. Water conduction through the hydrophobic channel of a carbon nanotube. *Nature* **2001**, 414, 188–190.
- (184) Ye, Y.-S.; Rick, J.; Hwang, B.-J. Water soluble polymers as proton exchange membranes for fuel cells. *Polymers* **2012**, *4*, 913–963
- (185) Tuckerman, M. E.; Ungar, P. J.; Vonrosenvinge, T.; Klein, M. L. Ab Initio Molecular Dynamics Simulations. *J. Phys. Chem. A* **1996**, 100, No. 12878.
- (186) Tuckerman, M.; Laasonen, K.; Sprik, M.; Parrinello, M. Ab Initio Molecular Dynamics Simulation of the Solvation and Transport of H3O+ and OH- Ions in Water. *J. Phys. Chem. A* **1995**, *99*, 5749.
- (187) Schmitt, U. W.; Voth, G. A. The computer simulation of proton transport in water. *J. Chem. Phys.* **1999**, *111*, 9361–9381.
- (188) Schmitt, U. W.; Voth, G. A. Multistate empirical valence bond model for proton transport in water. *J. Phys. Chem. B* **1998**, *102*, 5547–5551.
- (189) Kemp, M. T.; Lewandowski, E. M.; Chen, Y. Low barrier hydrogen bonds in protein structure and function. *Biochim. Biophys. Acta, Proteins Proteomics* **2021**, *1869*, No. 140557.
- (190) Frey, P. A.; Whitt, S. A.; Tobin, J. B. A Low-Barrier Hydrogen-Bond in the Catalytic Triad of Serine Proteases. *Science* **1994**, *264*, 1927.
- (191) Raghavachari, K.; Trucks, G. W.; Pople, J. A.; Head-Gordon, M. A fifth-order perturbation comparison of electron correlation theories. *Chem. Phys. Lett.* **1989**, *157*, 479–483.

- (192) Hammes-Schiffer, S. Theory of Proton-Coupled Electron Transfer in Energy Conversion Processes. *Acc. Chem. Res.* **2009**, *42*, 1881–1889.
- (193) Harris, D. F.; Lukoyanov, D. A.; Shaw, S.; Compton, P.; Tokmina-Lukaszewska, M.; Bothner, B.; Kelleher, N.; Dean, D. R.; Hoffman, B. M.; Seefeldt, L. C. The Mechanism of  $N_2$  Reduction Catalyzed by Fe-Nitrogenase Involves Reductive Elimination of  $H_2$ . Biochemistry **2018**, *57*, 701–710.
- (194) Mardirossian, N.; Head-Gordon, M. Thirty years of density functional theory in computational chemistry: an overview and extensive assessment of 200 density functionals. *Mol. Phys.* **2017**, *115*, 2315–2372.